The Institute of Paper Chemistry

Appleton, Wisconsin

Doctor's Dissertation

Two-Dimensional Flow of Fluids in Deformable Porous Media

Richard M. Peterson

January, 1969

TWO-DIMENSIONAL FLOW OF FLUIDS IN DEFORMABLE POROUS MEDIA

A thesis submitted by

Richard M. Peterson

B.S.Ch.E. 1964, The University of Wisconsin
M.S. 1966, Lawrence University

in partial fulfillment of the requirements
of The Institute of Paper Chemistry
for the degree of Doctor of Philosophy
from Lawrence University,
Appleton, Wisconsin

January, 1969

TABLE OF CONTENTS

SUMMARY

This study is an attempt to characterize the two-dimensional flow of a fluid through a deformable* porous material, specifically through a fiber mat. The complex nature of fibrous materials necessitates that the porous medium be considered both anisotropic and deformable.

A review of the literature on permeation of fibrous materials reveals that most studies have considered only flow perpendicular to the plane of the fiber mat. However, there are many practical cases where flow in more than one direction is occurring. There are other instances where it might be profitable to use flow through the mat in some direction other than that normally considered. Thus, the study of two-dimensional flow in fibrous materials should yield valuable information.

For this study, the basic fiber properties of specific surface area and specific volume were measured. Also determined were the compressibility characteristics of the fiber mat and the permeability functions governing flow in the mat in the two major directions. These basic fiber and fiber mat properties were then used in a numerical solution of the two-dimensional flow equation to predict the overall two-dimensional flow behavior of the experimental system.

The experimental results indicated that the permeability for flow in the lateral direction (parallel to the plane of the fiber mat) was 25 to 30% greater than the permeability for flow in the transverse direction (perpendicular to the plane of the mat). Thus, there is considerably less resistance to flow in the lateral direction. This graphically points out the anisotropic nature of fibrous materials.

*Deformable and compressible are used interchangeably in this study to indicate a medium in which the particles of the medium can be brought closer together, but the applied pressure is insufficient to change the actual density of the particles themselves.

Comparison of experimental data on two-dimensional flow with the predictions of the numerical solution indicated good agreement. Values of overall flow rate and pressure drop obtained by the two methods generally agreed within 1-2%. The slight deviations that were found could easily be explained and were generally due to simplifying assumptions made in developing the theory.

The theoretical results were also used to predict the relative importance of some of the factors governing two-dimensional flow. Of major importance in affecting overall flow results were the geometry of the system and the average porosity of the porous material. Changes in the porosity distribution within the porous medium were of less importance. The importance of considering the anisotropic nature of the fibrous medium was dependent on the relative amounts of transverse and lateral flow.

Thus, this study accomplished three main objectives. (1) It characterized the anisotropic permeabilities of a fibrous material with the fibers oriented randomly in the x-y plane. (2) It provided a numerical solution of the two-dimensional flow equation which adequately described the two-dimensional flow occurring in the experimental system. (3) The numerical solution also provided a useful indication of the relative importance of several factors governing two-dimensional flow in deformable porous media.

INTRODUCTION AND LITERATURE REVIEW

PERMEABILITY RELATIONSHIPS

The flow of fluids through porous media has been the subject of extensive study in the past. As early as 1856, Darcy found that the rate of flow Q of water through a sand filter bed was directly proportional to the cross-sectional area of the bed A and to the pressure difference across the bed ΔP and inversely proportional to the thickness of the bed L.

$$Q = K \frac{A\Delta P}{L} \tag{1}$$

Much of the work that followed was an attempt to discover the nature of the permeability coefficient K. One of the earliest discoveries was that the flow rate was inversely proportional to the viscosity μ of the permeation fluid. This allowed Darcy's relationship to be written in the form

$$Q = \frac{K'}{\mu} \frac{A\Delta P}{L} . \tag{2}$$

In this form, the permeability K' is dependent only on the nature of the porous medium.

HYDRAULIC RADIUS THEORIES

The void volume or porosity ε of the porous medium was known to influence the permeability. Slichter, in 1897, considered a granular bed as an equivalent system of capillary tubes and found the permeability as an empirical function of the porosity and a characteristic dimension of the porous material (average diameter of the granules). Kozeny (1) made a valuable contribution when he observed the similarity between Darcy's equation and Poiseuille's expression for the streamline flow of fluids through straight cylindrical pipes. Generalizing Poiseuille's

equation by the introduction of a hydraulic radius and comparing with Darcy's equation, Kozeny found the permeability to be dependent on porosity and on the specific surface area S_v of the particles of the porous medium. Carman (2) later expanded on this relationship and obtained the well-known Kozeny-Carman equation

$$Q = K \frac{A \cdot \Delta P}{L} = \frac{\varepsilon^3}{k \mu S_{v^2} (1-\varepsilon)^2} \frac{A \cdot \Delta P}{L} . \qquad (3)$$

This equation seemed to be an excellent fit for most of the data available at that time. It still contained an unknown function, the Kozeny factor k, but this appeared to be a constant for the low to medium porosity materials that were being investigated at that time. However, by the early 1940's, Sullivan and Hertel (3,4) found that k did not remain constant for flow through highly porous fiber beds. They introduced an orientation function into the Kozeny factor so that k varied from about three to six, depending on whether the axes of the fibers were oriented parallel or perpendicular to flow. They also found a complete breakdown of the Kozeny-Carman equation at porosities greater than 0.9.

DRAG THEORIES

At the same time that Kozeny was developing his hydraulic radius theory, Emersleben (5) attempted a mathematical solution of the hydrodynamic problem of the viscous drag of a fluid on a special array of parallel fibers. Burke and Plummer (6) later used the drag on spheres to obtain an equation for the dependence of the permeability of a porous medium on porosity. These drag theories led to different expressions for the dependence of permeability on porosity than that given by the hydraulic radius theory. Because existing data at that time and later (particularly on flow through sands) appeared to be consistent with the hydraulic radius theory, little attention was given to the drag theories.

The later discovery, however, that the hydraulic radius theory seemed to break down at high porosities, awakened renewed interest in the drag theories because they should be particularly applicable at high porosities. Iberall (7), working with highly porous glass wool, used the drag theory to derive an expression for flow through porous materials. He reported that his experimental data could be fitted to an equation of this type with a slight modification of the numerical constants, representing reasonable changes in the amount and relative weighting of the parallel and perpendicular fiber drags. Starting with the Navier-Stokes equations, Happel (8) obtained theoretical expressions for creeping flow parallel and perpendicular to cylinders. His results indicated that less resistance is offered to flow parallel to the cylinders than to flow perpendicular to the cylinders. Happel's theoretical curves were found to bound the actual experimental data for flow through fiber beds.

EMPIRICAL RELATIONSHIPS

In addition to the theoretical work, there were many attempts to obtain empirical correlations to describe the experimental data. Davies (9), in dealing with air flow through fibrous materials, formed a dimensionless group from elements of the Darcy equation along with the mean fiber radius and found a unique relationship between the bed porosity and this group. After conversion into consistent units, his empirical function yielded the following expression for the Kozeny factor $\underline{k}$:

$$k = \frac{k_1 \, \varepsilon^3}{(1-\varepsilon)^{1/2}} \left[1 + k_2(1-\varepsilon)^3\right] \qquad (4)$$

where

$\underline{k}_1 = 4.0$

$\underline{k}_2 = 56$

Ingmanson (10) correlated water permeability measurements on glass and nylon fibers and confirmed Davies' relationship with $\underline{k}_1 = 3.5$ and $\underline{k}_2 = 57$. He attributed the

slight variation in the constants to differences in the average fiber orientation in their respective mats.

One of the problems with the above correlations is that at low porosities they yield rapidly decreasing values of the Kozeny factor $\underline{k}$. However, it has been amply demonstrated that the Kozeny factor remains nearly constant at low porosities. To overcome this shortcoming, Carroll (11) proposed the following correlation for $\underline{k}$:

$$k = 5.0 + \exp[14(\varepsilon - 0.8)]. \qquad (5)$$

This correlation fitted the experimental data better over the whole experimental range than did the Davies-type correlation. However, at high porosities, the Davies-Ingmanson correlation best described the experimental data of this study.

COMPARISON OF THE PERMEABILITY RELATIONSHIPS

Neither of the two major theories describes the permeability characteristics of all porous materials. The conditions assumed in deriving the respective theories must be considered. The hydraulic radius theory appears valid at low to medium porosities where the assumption of a connected series of flow channels approximates the true situation. The drag theory appears to apply at high porosities where the resistance to flow can be computed as the sum of the fluid drags on each element and interaction among adjacent elements is small. In the region in between, neither may be fully applicable.

A comparison of the empirical relationships with the hydraulic radius and drag theories is shown in Fig. 1. The drag theory is represented by Happel's results for flow parallel and perpendicular to arrays of cylinders. It is seen that these results bracket the empirical correlations. The hydraulic radius theory is represented by the horizontal line at approximately $\underline{k} = 5.5$ ($\underline{k}$ is a constant, independent of porosity). At the lower porosities, this is a good approximation; however, at

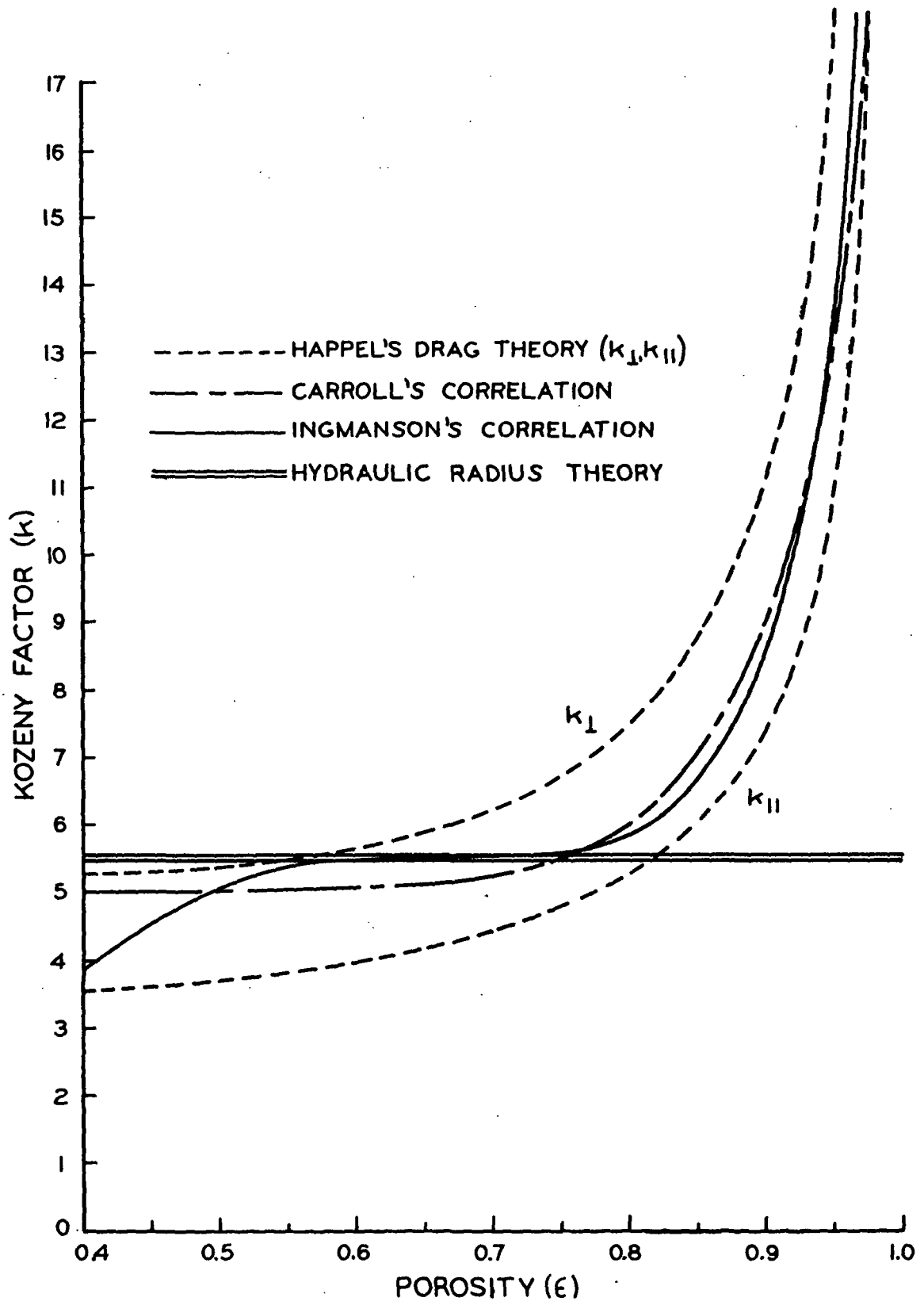

Figure 1. Kozeny Factor Correlations

porosities greater than about 0.75, the actual results begin to deviate widely from the theoretical prediction. The rapid decrease in the Kozeny factor at lower porosities for the Davis-Ingmanson type correlation is readily apparent in Fig. 1. But this is not believed to be a serious disadvantage because rarely, if ever, are porosities below 0.6 encountered in work with wet fibrous systems. Thus, it is often acceptable and more convenient to use this correlation rather than Carroll's three-parameter formula.

COMPRESSIBILITY RELATIONSHIPS

In beds composed of rigid, noncompressible particles the permeability relationships reviewed in the preceding section are sufficient to describe slow fluid flow. However, in deformable beds, the fluid drag forces tend to compress the bed so that the compression response of the mat must also be known.

Several investigators have studied the static compressibility of fibrous mats. In these experiments, a uniform compacting load was applied to unbonded, water-saturated fiber mats. Campbell (12) related the mat concentration c to the applied pressure P_f with the following simple relationship for first compression data:

$$c = M P_f^N \tag{6}$$

where M and N are compressibility constants.

At very low applied pressures, this equation predicts mat concentration approaching zero, which is physically impossible. To correct for this deficiency, three-parameter models have been proposed to describe the compression response. Ingmanson (13) introduced a model of the form

$$c - c_o = M' P_f^{N'} \tag{7}$$

while Wilder's model (14) took the form

$$c^{\gamma} - c_o^{\gamma} = M_o P_f \qquad (8)$$

Here c_o is the mat density at zero applied load. The value of c_o has not been precisely determined. However, various authors (13-16) have estimated the solid fraction $(1-\varepsilon) = c_o v$ at zero applied load to range from 0.02 to 0.04. From the correlation of much applied data, it appears that Wilder's equation is slightly superior to Ingmanson's at very low loads.

The values of the compressibility constants M and N were found to be dependent on fiber properties. Han's (17) analysis of experimental data in light of Wilder's compressibility function indicated that the modulus of elasticity of the fibers was of prime importance. Experimental studies, such as that by Jones (15), indicated that for cylindrical fibers, M and N increased with increasing axis ratio (length-diameter) until a critical value was reached. Beyond this point, they were found to be constant. Jones also found that fiber curl caused increased values of N. This could be the reason that wood pulp fibers generally have higher N values than synthetic fibers which are normally fairly straight.

Many factors complicate the measurement of mat compressibility. At any time during compression, if the load is decreased, the mat loosens, but never recovers to the full extent corresponding to the original lower compression. If the load if reapplied, the deformation in the second compression will be less than that of the first. Thus, the compression-recovery cycles exhibit hysteresis. According to Jones (15), the nonrecoverable deformation arises primarily from repositioning of the fibers due to slippage. If these hysteresis effects are to be avoided, all compressibility experiments must be run under conditions of increasing load. Fiber mats also exhibit creep when under compression. To eliminate the effects of creep, all mat density readings must be taken at the same time after the application of

the load. Vibrations can also cause an effect by mechanically conditioning the mat, resulting in a more highly compressed mat. Wall effects, due to considerable Z-orientation near the wall, can also be of importance.

ONE-DIMENSIONAL FLOW INVESTIGATIONS

The majority of the investigations of fluid flow through porous media have been concerned with flow in only one principal direction through the medium. All of the permeability investigations discussed earlier were of this type. The earliest investigations considered only flow through nondeformable media. For these studies, the simplest form of Darcy's law [Equations (1) or (2) with a constant permeability K] applied. Later investigations dealt with increasingly more complex problems such as filtrations of nondeformable media, flow through deformable media, and filtration of deformable media.

DEFORMABLE MEDIA

The introduction of a deformable medium complicated the analysis because the fluid drag forces caused a variation of porosity and thus of permeability throughout the mat. Thus, permeability had to be considered a local property of the mat and not a constant. Much early work with flow through deformable fibrous mats was done at The Institute of Paper Chemistry by Ingmanson, both by himself (18,19) and in conjunction with other members of the staff (13,20). Much of this early work sought to describe an average filtration resistance of the deformable fibrous mats. Later work by Ingmanson (10) and by many other authors (21-26) dealt with the measurement of the internal pressure and porosity distributions within the mats. Tiller and Huang (27) and Ingmanson (28) reported that a further complication occurred in the filtration of high-consistency fiber suspensions. They found more water leaving the bottom surface of the mat than entering at the top. This was due to a

squeeze-out of the water within the mat by the compressive forces acting on the mat. The result was a velocity distribution within the mat which altered the porosity distribution. Summarizing much of the above work, Meyer (29) presented a general filtration theory for compressible fibrous beds formed from dilute suspensions.

INERTIAL EFFECTS

In 1963, Ingmanson and Andrews (30) reported on a study of the high-velocity flow of water through fiber beds. They found that for this type of flow, where the inertial forces were not negligible, the Forchheimer formula could be used to describe the flow.

$$\frac{\Delta P}{L} = a|u| + bu^2 \qquad (9)$$

Here a and b are the viscous and inertial resistances, respectively. When the flow is slow, the viscous effect predominates and Forchheimer's formula reduces to Darcy's law. For high flow rates the quadratic term representing the inertial losses predominates. Nelson (31) presented a general filtration theory in which he suggested a method of accounting for resistance to flow when the solid phase is in motion. This article covered most of the work done with one-dimensional flow through porous media up to the present time.

MULTIDIMENSIONAL FLOW

ISOTROPIC, NONDEFORMABLE MEDIA

Compared to one-dimensional flow, there have been relatively few studies of two- or three-dimensional flow through porous media. The majority of the work in this area has been done by geologists studying the flow of ground water or oil through porous rocks or soil into wells. Since most of these materials are fairly stable, these studies have generally considered only nondeformable media. Both

Muskat (32) and Scheideggar (33) have dealt extensively with such flow in their texts. Muskat showed that by combining Darcy's law with the equation of continuity, the Laplace equation is obtained.

$$\nabla^2((K/\mu)P) = (K/\mu)\nabla^2 P = 0$$

or

$$\nabla^2 P = 0. \qquad (10)$$

This equation applies to the creeping flow of an incompressible fluid through an isotropic, nondeformable medium.

Potential theory and conformal mapping were generally used to solve the Laplace equation for the specific boundary conditions of the system in question. Muskat (32) and Streeter (34) gave several examples of the application of potential theory and conformal mapping to flow through porous media. Engelund (35), studying the flow of ground water in homogeneous sands, was able to solve the Laplace equation for two-dimensional flow and confirmed his solution with experimental measurements. Likewise Kirkham (36) obtained a more exact solution of the Laplace equation for similar boundary conditions. Brenner (37) studied the three-dimensional filtration of a nondeformable material. His experimental results deviated slightly from that theoretically predicted and he attributed this to a slight filter cake compressibility, which was neglected in the theoretical equation.

ANISOTROPIC AND DEFORMABLE MEDIA

Although such materials as soil and rock are usually nondeformable, they are not always isotropic. Johnson and Hughes (38) carried out directional permeability measurements on core samples and found marked permeability differences between the horizontal and vertical planes of many samples. Muskat (32) indicated, however, that by transforming the coordinate system, an equation of Laplace's form could be

obtained to describe such anisotropic systems. Then it is possible to solve such a problem in the conventional way.

There have been very few studies on multidimensional flow through deformable media. A theory covering the consolidation of an anisotropic deformable solid has been developed by Biot (39,40) and applied to fluid flow by Paria (41). The variation of porosity within such a deformable system made the problem too complex to solve by other than numerical means. Thus, until the relatively recent development of high-speed computers, there has been no opportunity to solve the theoretical predictions and compare them with experimental data.

STATEMENT OF THE PROBLEM

A fibrous material is a complex system which is both anisotropic and deformable. The preceding literature review has shown that the majority of the work to date on fibrous systems has been concerned with only one-dimensional superficial flow perpendicular to the plane of the fiber mat. (Flow in this direction will hereafter be referred to as transverse flow. Flow in the plane of the mat will be called lateral flow.) However, in many practical situations, flow within a fibrous material is not merely one-dimensional, but rather is multidimensional in nature. Thus, it becomes important to be able to describe this multidimensional flow and determine how it is affected by the anisotropy and deformability of the medium.

The development of computers has now made it possible to solve numerically the mathematical equations governing the multidimensional flow of fluids through deformable porous media. To facilitate this solution, this study makes use of a two-dimensional model without any great loss of generality. The experimentally determined permeability functions in the two major directions (transverse and lateral) are combined with a two-dimensional form of Darcy's law and a compressibility function to describe theoretically the two-dimensional creeping flow in an anisotropic, deformable medium. This mathematical expression is then solved numerically for the boundary conditions of the experimental system and the theoretical predictions are compared with the experimental results.

While the numerical solution of the mathematical equation is useful in describing experimental conditions, it is also extremely helpful in predicting the effect of a change in the experimental conditions on the final solution. Thus, an important sidelight to this study is the valuable information obtained by observing the relative importance of the change of such conditions as: (1) porosity, (2) permeability, (3) degree of anisotropy, (4) geometry of the system, and (5) deformability.

MATHEMATICAL TREATMENT OF TWO-DIMENSIONAL FLOW THROUGH DEFORMABLE POROUS MEDIA

THEORETICAL DEVELOPMENT OF TWO-DIMENSIONAL FLOW EQUATIONS

While this study is only concerned with two-dimensional flow under certain restricted conditions, it is helpful to derive the mathematical equations pertaining to the most general case of three-dimensional flow. Then these equations will be simplified to the final form. In this way the assumptions made in deriving the final equations are evident and the limitations of the equations are readily apparent.

Biot (39,40) and Paria (41) indicate that Darcy's law may be written for three cartesian coordinates in the following form:

$$-\begin{Vmatrix} u_x \\ u_y \\ u_z \end{Vmatrix} = \begin{Vmatrix} K_{xx} & K_{xy} & K_{xz} \\ K_{yx} & K_{yy} & K_{yz} \\ K_{zx} & K_{zy} & K_{zz} \end{Vmatrix} \cdot \begin{Vmatrix} \frac{\partial P}{\partial x} \\ \frac{\partial P}{\partial y} \\ \frac{\partial P}{\partial z} \end{Vmatrix} \tag{11}$$

or

$$\begin{aligned} -u_x &= K_{xx}\frac{\partial P}{\partial x} + K_{xy}\frac{\partial P}{\partial y} + K_{xz}\frac{\partial P}{\partial z} \\ -u_y &= K_{yx}\frac{\partial P}{\partial x} + K_{yy}\frac{\partial P}{\partial y} + K_{yz}\frac{\partial P}{\partial z} \\ -u_z &= K_{zx}\frac{\partial P}{\partial x} + K_{zy}\frac{\partial P}{\partial y} + K_{zz}\frac{\partial P}{\partial z}\,. \end{aligned} \tag{12}$$

Also, the equation of continuity states that

$$\frac{\partial u_x}{\partial x} + \frac{\partial u_y}{\partial y} + \frac{\partial u_z}{\partial z} = 0. \tag{13}$$

Then the combination of Darcy's law and the equation of continuity yields the general equation for the three-dimensional flow of a fluid through a deformable porous medium.

$$\frac{\partial}{\partial x}\left[K_{xx}\frac{\partial P}{\partial x}+K_{xy}\frac{\partial P}{\partial y}+K_{xz}\frac{\partial P}{\partial z}\right]$$

$$+\frac{\partial}{\partial y}\left[K_{yx}\frac{\partial P}{\partial x}+K_{yy}\frac{\partial P}{\partial y}+K_{yz}\frac{\partial P}{\partial z}\right] \qquad (14)$$

$$+\frac{\partial}{\partial z}\left[K_{zx}\frac{\partial P}{\partial x}+K_{zy}\frac{\partial P}{\partial y}+K_{zz}\frac{\partial P}{\partial z}\right]=0.$$

However, in the experimental system, flow occurs in only two directions. Thus, considering only flow in the transverse or z-direction and in the lateral or x-direction, the equation becomes

$$\frac{\partial}{\partial x}\left(K_{xx}\frac{\partial P}{\partial x}+K_{xz}\frac{\partial P}{\partial z}\right)+\frac{\partial}{\partial z}\left(K_{zx}\frac{\partial P}{\partial x}+K_{zz}\frac{\partial P}{\partial z}\right)=0. \qquad (15)$$

To further simplify this equation, the terms containing the cross-permeabilities K_{xz} and K_{zx} will be neglected. These terms are identically equal to zero for random orientation of the fibers in the x-y plane. This is approximately true for the undeformed system because of the method of formation. If the fiber axes are tipped due to deformation, then these terms are nonzero. However, for the present experimental system which is precompressed to a large degree, this effect should be minimal and the cross terms can probably be safely neglected when compared to the magnitude of the other terms. The deviation of the final solution from the experimental results should give an indication of the validity of this assumption. The final simplified form of the equation for two-dimensional flow of a fluid through a deformable porous medium is thus

$$\frac{\partial}{\partial x}\left(K_{xx}\frac{\partial P}{\partial x}\right)+\frac{\partial}{\partial z}\left(K_{zz}\frac{\partial P}{\partial z}\right)=0 \qquad (16)$$

or

$$\frac{\partial K_{xx}}{\partial x}\frac{\partial P}{\partial x}+K_{xx}\frac{\partial^2 P}{\partial x^2}+\frac{\partial K_{zz}}{\partial z}\frac{\partial P}{\partial z}+K_{zz}\frac{\partial^2 P}{\partial z^2}=0. \qquad (17)$$

If the medium is anisotropic, but not deformable, so that $\underline{\underline{K}}_{xx}$ and $\underline{\underline{K}}_{zz}$ are constant, then the equation can be further simplified to

$$K_{xx} \frac{\partial^2 P}{\partial x^2} + K_{zz} \frac{\partial^2 P}{\partial z^2} = 0. \tag{18}$$

Finally, if the medium is completely isotropic and nondeformable, then the equation reduces to the two-dimensional Laplace equation.

$$\frac{\partial^2 P}{\partial x^2} + \frac{\partial^2 P}{\partial z^2} = 0 \tag{19}$$

Analytical solutions of these partial differential equations [particularly Equations (16) or (17)] are difficult without making many limiting assumptions. Thus, to get meaningful results, numerical techniques must be used. The use of finite difference methods has been found satisfactory for similar flow problems and will be used in this study. A detailed discussion of how the finite difference method was applied to this system will be found in Appendix I. The final finite difference equations obtained for Equations (17)-(19) are summarized in Table I.

Also necessary for the numerical solution of these partial differential equations are certain supplementary conditions. These include the boundary and initial conditions and the permeability and compressibility relations. These functions describe the relationship between pressure, porosity, and permeability within the mat. Pressure on the fibers caused by fluid drag forces causes changes in the porosity within the fiber mat, which in turn results in changes in the permeabilities. The porosity-permeability relationship used in this study was the Kozeny-Carman equation [Equation (3)] with the Davies-Kozeny factor correlation [Equation (4)]. Campbell's compressibility function [Equation (6)] was used to relate porosity and compressive pressure on the fibers. The application of these functions in this study is discussed in greater detail in Appendix I.

TABLE I

FINITE DIFFERENCE FLOW EQUATIONS

Flow Through Deformable Porous Media:

$$1/4\ [(K^x_{i+1,j} - K^x_{i-1,j})\cdot(P_{i+1,j} - P_{i-1,j})$$

$$+ (K^z_{i,j+1} - K^z_{i,j-1})\cdot(P_{i,j+1} - P_{i,j-1})]$$

$$+ K^x_{i,j}\ (P_{i+1,j} - 2P_{i,j} + P_{i-1,j})$$

$$+ K^z_{i,j}\ (P_{i,j+1} - 2P_{i,j} + P_{i,j-1}) = 0$$

Flow Through Anisotropic Porous Media:

$$K^x\ (P_{i+1,j} - 2P_{i,j} + P_{i-1,j})$$

$$+ K^z\ (P_{i,j+1} - 2P_{i,j} + P_{i,j-1}) = 0$$

Flow Through Isotropic Porous Media:

$$P_{i+1,j} + P_{i-1,j} + P_{i,j+1} + P_{i,j-1} - 4P_{i,j} = 0$$

The result of applying the finite difference iteration procedure to the model system was a set of pressure values representing the pressure distribution within the porous medium. A data mapping program developed by Perry (42) was slightly modified and used to obtain plots of the pressure distributions within the porous media. These plots are not precisely accurate because of linear interpolation between data points, but they do give a good general description of the pressure distributions. Such a plot is shown in Fig. 2.

This figure represents one-half of the fiber mat, cut down the middle. The upper surface represents the open face of the mat, while the slot is in the lower

right-hand corner. Each line within the mat represents a drop of one-tenth of the total pressure drop across the mat. Thus, if the overall pressure drop is ten centimeters of water, then the drop between two successive lines is one centimeter of water. (The slight irregularities shown in Fig. 2 result from the data mapping program and do not reflect irregularities in the data. All numerical calculations were performed using the basic data.)

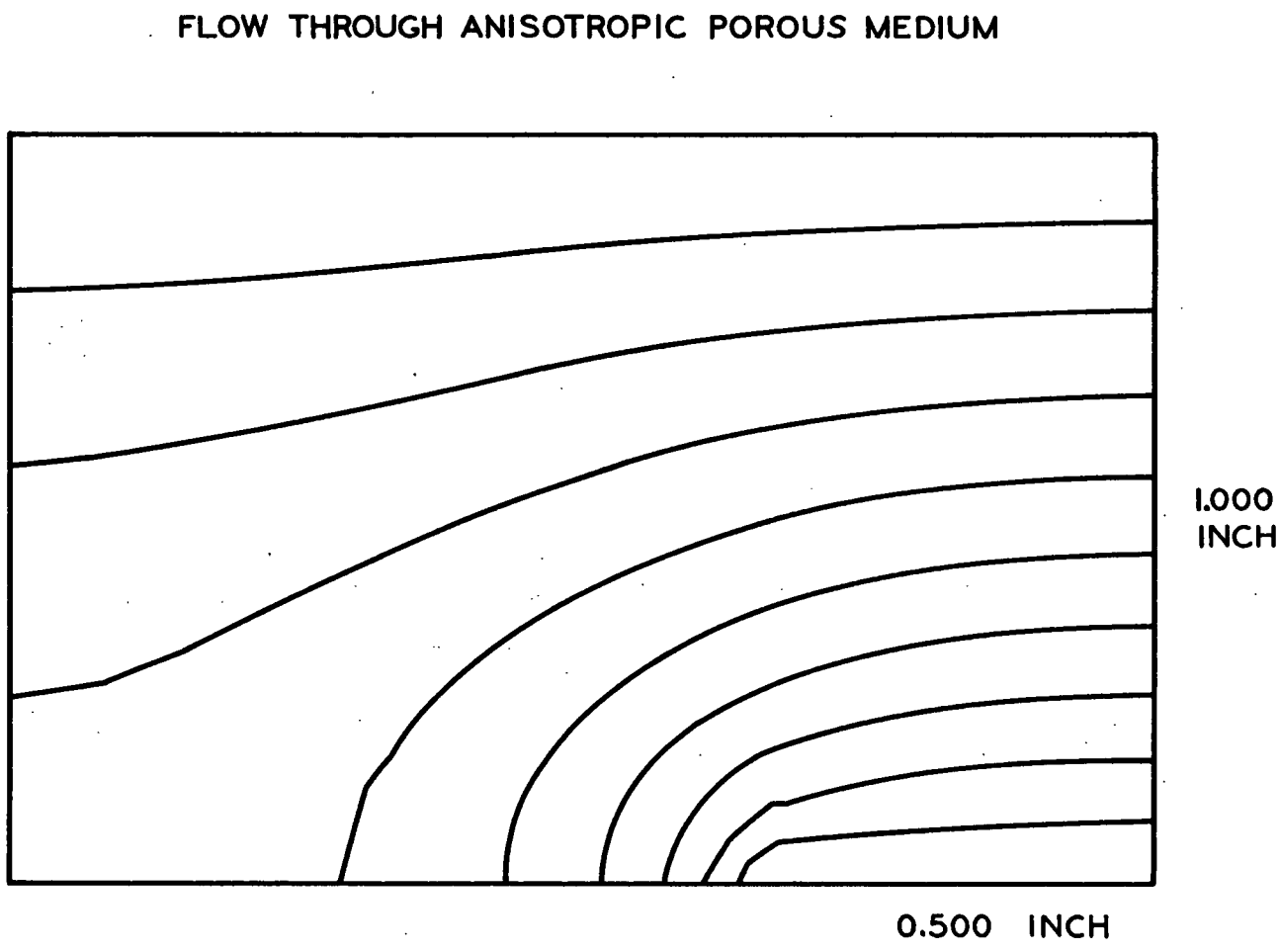

Figure 2. Pressure Distribution in a Fiber Mat

DEVELOPMENT OF OVERALL PRESSURE DROP-FLOW RATE EXPRESSIONS

Numerical solution of the two-dimensional flow equations derived above yields a set of pressure drop values representing the pressure distribution in the porous

medium. However, the solution in this form is not immediately very useful because of the experimental difficulty of measuring such a pressure distribution in a fiber mat. Experimentally, the values of the overall pressure drop and flow rate are most easily obtained. Thus, the pressure distributions obtained from the computer must be converted into some kind of overall data.

This conversion can be accomplished quite easily. First, the z-component of the velocity at any point can be represented by the equation

$$u_z = -K_{zz} \frac{\partial P}{\partial z} . \qquad (20)$$

This equation is then transformed into a difference equation and solved numerically at each lattice point. Then these velocity values are numerically integrated at a constant value of z within the mat to obtain the overall volumetric flow rate Q in the z-direction. This overall flow rate, along with the overall pressure drop which was imposed on the solution of the pressure distribution as a boundary condition, provide the necessary overall theoretical data.

EXPERIMENTAL APPARATUS AND PROCEDURES

The experimental program consisted of three main parts. These included (1) the measurement of fundamental fiber and fiber mat properties, (2) the characterization of two-dimensional flow through an isotropic medium, and (3) the characterization of two-dimensional flow in an anisotropic, deformable medium.

FUNDAMENTAL FIBER AND FIBER MAT PROPERTIES

The basic properties of both the individual fibers and of the fiber mat were determined experimentally. These properties were needed for substitution into the theoretical equations. With these basic parameters, the theoretical equations could be solved and then compared with the experimental results for two-dimensional flow through the fibrous system.

FIBERS

The selection of the correct fiber in such a study is extremely critical. It is desired to choose a system as close to the natural system as possible without introducing factors which would complicate the interpretation of the final results. Of course, the use of wood pulp fibers would give the most realistic simulation of a real system. However, there are many characteristics of such fibers which would make any experimental results most difficult to analyze. These include hollow lumens leading to collapse, swelling in water, irregular cross sections, non-uniform lengths and diameters, and a general heterogeneous nature. Experience has shown that the use of inert, cylindrical fibers allows reproducible results and avoids many of the complications introduced by wood pulp fibers. Nylon, dacron, and glass fibers have been used in earlier investigations with good results. Because of the tendency of glass fibers to shatter under compressive loading, dacron and

nylon fibers were considered for this study. Since better formation was obtained with the nylon fibers, these were finally selected.

Of the basic fiber properties needed for this study, the specific surface and specific volume were most important. For solid cylindrical fibers, the specific surface can be determined microscopically (it is a function of fiber diameter) and the specific volume is equal to the reciprocal of the fiber density.

FIBER MAT COMPRESSIBILITY

For flow through deformable media, the compressibility of the mat is an important function which must be determined. Measurement of fiber mat compressibility is a routine procedure whereby a fiber mat is compacted with known pressures and the mat concentration is determined. Ingmanson and Whitney (13) reported that such experimental deformability data can be fitted with good precision by an empirical function of the form

$$c = M P_f^N \tag{6}$$

where M and N are the compressibility constants. These constants were determined experimentally for this system in the above-described manner.

FIBER MAT PERMEABILITY

The final fiber mat property needed is the mat permeability. In an anisotropic material such as a fiber mat, the permeability is a directional property and thus must be determined in both of the two principal directions. Thus, if the fiber axes lie in the x-y plane, the in-plane or lateral permeability and the cross-plane or transverse permeability must both be measured.

Figure 3 is a schematic drawing of the overall flow system used for forming the fiber mat and then for making the permeability measurements. Figure 4 shows

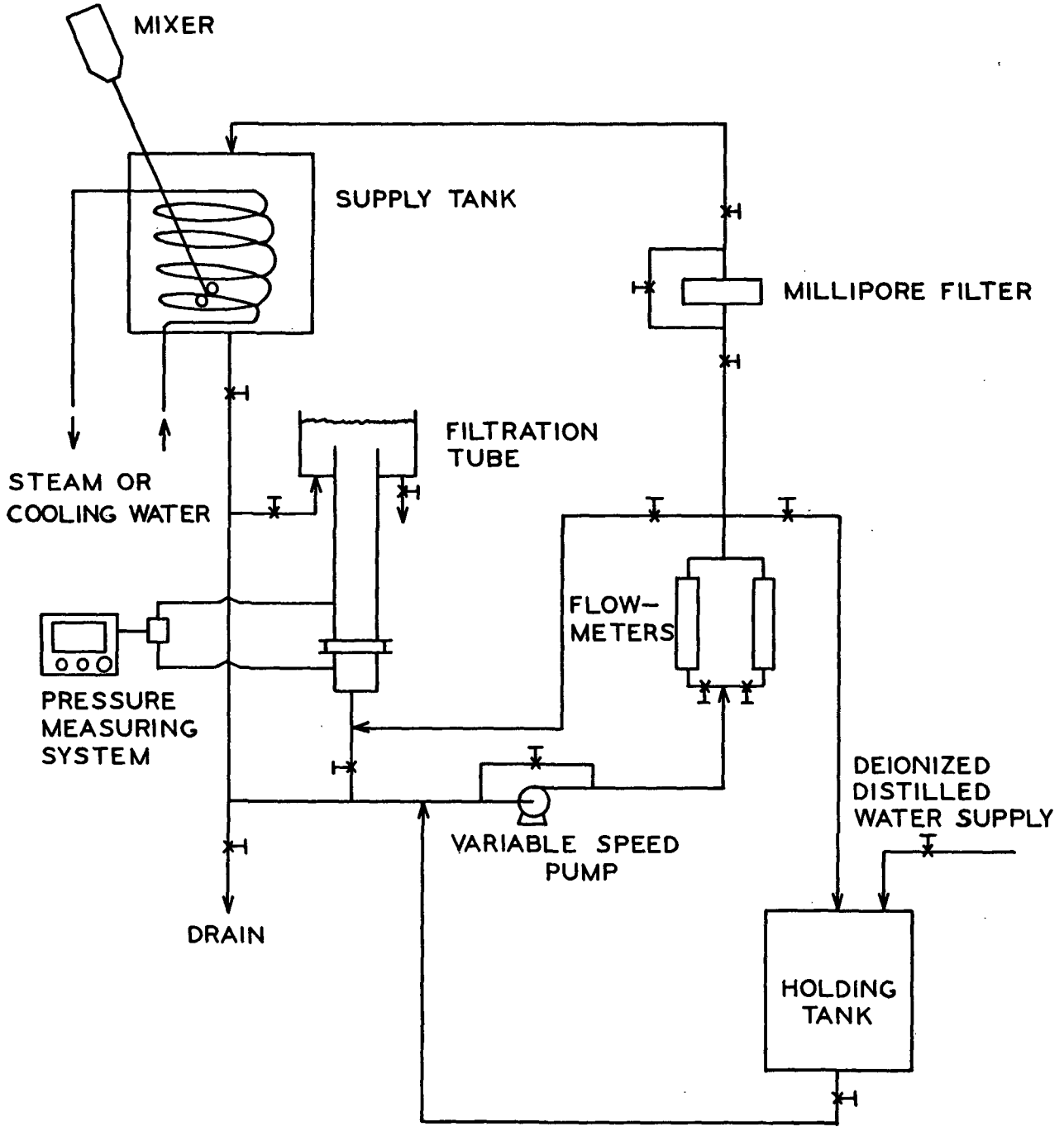

Figure 3. Overall Flow System

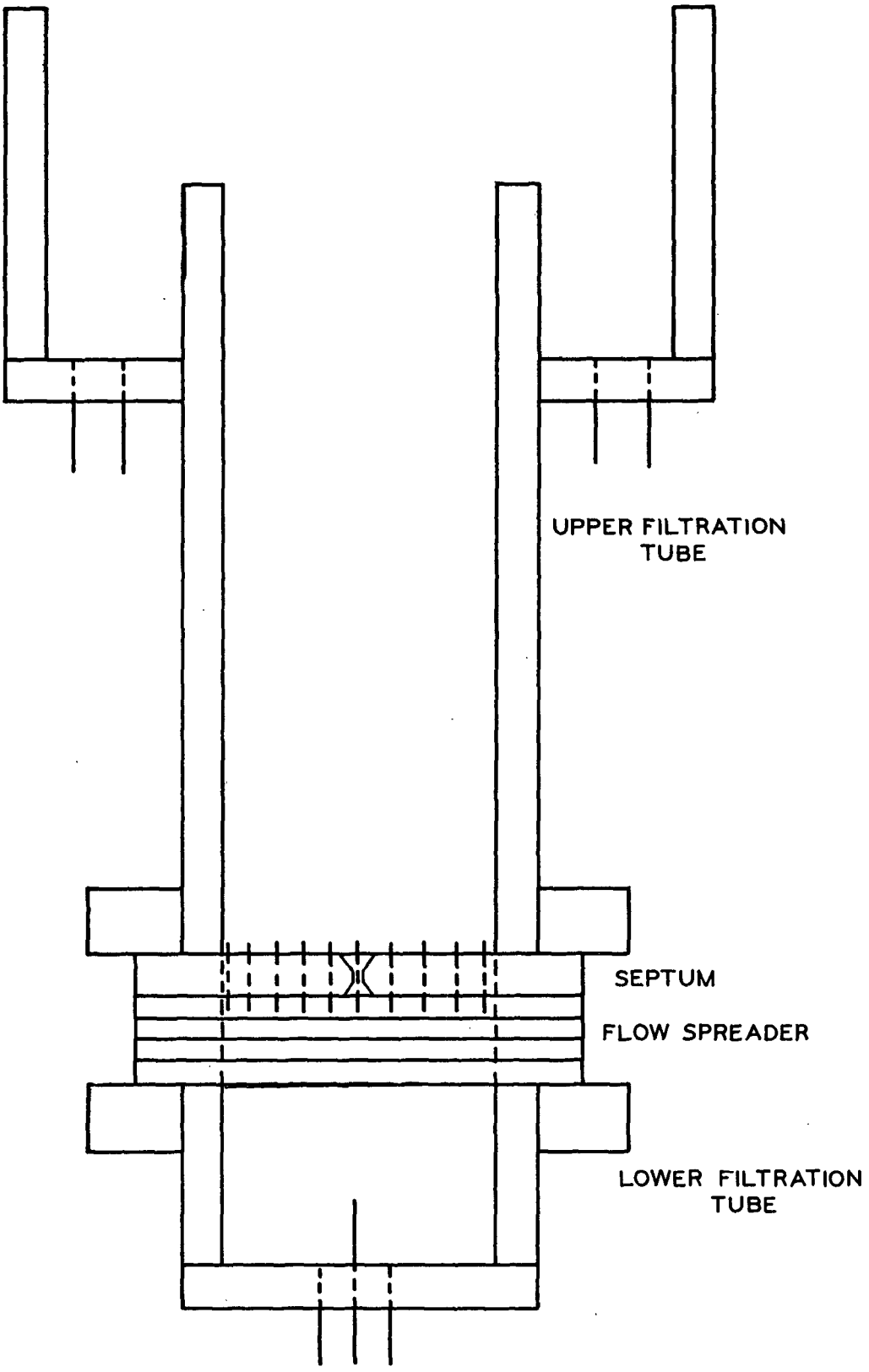

Figure 4. Filtration Tube

the filtration tube, the most important component of this system. The filtration tube has a square cross section, three inches on a side. This design was chosen to facilitate the measurement of the lateral permeability. The septum is a drilled and countersunk brass plate covered with 65- and 100-mesh brass screens. The flow spreader is made of three 65-mesh brass screens to insure a uniform distribution of fluid velocities across the mat.

Mat Formation

The first step in the permeability measurements was to obtain a uniform fiber mat. In this procedure [refer to Fig. 3] deionized, distilled water was pumped through a Millipore filter into an elevated supply tank. This water was boiled to deaerate it and then cooled to room temperature. Next nylon fibers were added to make a dilute suspension (consistency approximately 0.001%). This suspension flowed by gravity into the upper section of the filtration tube and the fibers were collected on the septum. Because of the very low consistency, almost complete x-y orientation was obtained except for fibers close to the edge of the tube. Water was removed from the bottom of the filtration tube by a variable speed pump and returned through the Millipore filter back to the supply tank. Additional fibers were periodically added to the supply tank to maintain the consistency. In this way, a fiber mat with any desired total mass of fibers could be formed.

Transverse Permeability

For the permeability measurements, a permeable brass piston was lowered onto the surface of the formed fiber mat. Mat thickness was measured with a cathetometer. From these measurements, along with the weight of the fibers in the mat, the porosity was determined. During the permeability runs, fresh deaerated, distilled water from the supply tank flowed through a flowmeter and then up through the bottom of the filtration tube. To determine the permeability, values of pressure drop versus

flow rate were recorded for a series of increasing flow rates. Plotting of these data resulted in a straight line [see Fig. 27 in Appendix V], and the permeability and Kozeny factor could be determined from the slope of this line. Normally duplicate runs were made at each porosity. Very low flow rates were used for these measurements so that the pressure drop due to flow was small compared to the mechanical pressure applied by the piston. In this way an approximately constant porosity throughout the fiber mat was assured. The pressure drops across the fiber mats were obtained by subtracting the pressure drop across the septum and permeable piston from the total pressure drop. This assumes that for thick mats, any mat-wire interaction is negligible, which has been well documented. Pressure drop measurements in the above procedure were made with a PACE Engineering Company differential pressure transducer. Details of the pressure measuring system are given in Appendix II.

The above procedure was then repeated on the same fiber mat by compressing it to a lower porosity. In this way, transverse permeability measurements were obtained for porosities ranging from about 0.75 to 0.96.

Lateral Permeability

Lateral permeability measurements were made in the same way as the transverse measurements, but the apparatus used was slightly different. Figure 5 shows the lateral permeability insert in the filtration tube. During formation, thin Plexiglas sheets were inserted in the filtration tube to cover up the side screens. These were removed after formation and a nonpermeable piston was lowered onto the top of the mat. Then water was forced sideways (laterally) through the mat and pressure drop-flow rate measurements were taken in the usual manner. From these measurements, lateral permeability and Kozeny factors were determined.

The main problem in this procedure was obtaining a seal at the top and bottom of the mat so leakage could not occur. First, an impermeable piston raised from the

bottom of the filtration tube to block the bottom of the mat was tried, but this proved unsatisfactory. The final solution was to seal off the top of the filtration tube and then let air up under the septum at the bottom. This air did not penetrate into the mat and effectively sealed off the bottom so leakage could not occur.

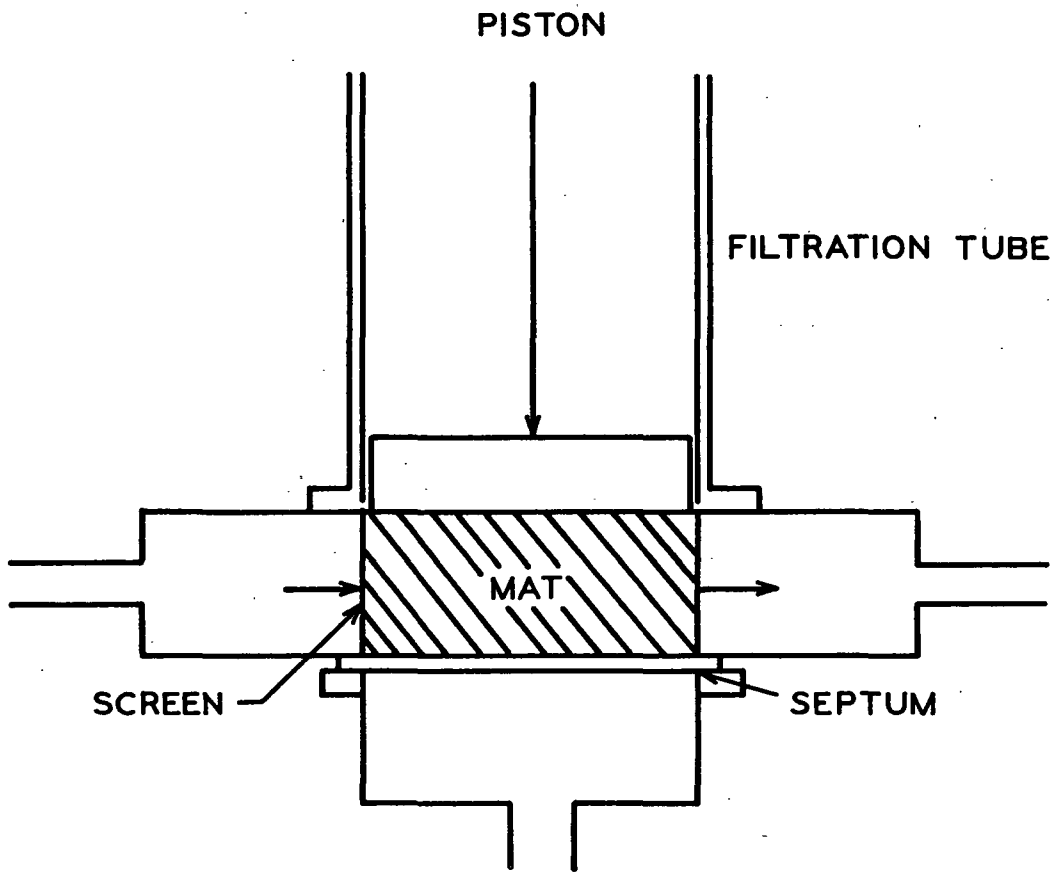

Figure 5. Lateral Permeability Apparatus

The lateral permeability could only be determined for one porosity at a time because the mat thickness had to be maintained at a constant value. Thus, to change the porosity, a new mat had to be formed with a different fiber weight. The pressure drop across the side screens was found to be negligible so no pressure drop corrections were made.

TWO-DIMENSIONAL FLOW STUDIES

The two-dimensional flow studies were also carried out in the filtration tube. To create a two-dimensional flow system, a slotted piston was lowered onto the surface of the porous medium. Then permeation water was forced upward through the open septum, through the porous medium, and finally through the slot. As seen in Fig. 6, this created flow in both major directions (transverse and lateral). Overall pressure drop and flow rate measurements were then made in the usual manner.

ISOTROPIC MEDIA

Two-dimensional measurements on isotropic media were taken first, mainly to check out the experimental system. Since theoretical predictions and experimental results had already been obtained on similar systems by Engelund (35), this provided a ready means of checking the experimental results.

A thick bed (21.5 cm.) of glass beads (20-40 mesh) was used as the isotropic medium. The permeability of the bed was determined from pressure drop-flow rate data using the permeable piston. Then three different slotted pistons (1, 1/2, 1/4-inch slot widths) were used to obtain varying degrees of two-dimensional flow. These results were then compared to those obtained by Engelund.

DEFORMABLE MEDIA

For the experiments with deformable media, the fiber mats were formed as described earlier. Then a slotted piston was lowered onto the mat surface and the mat was compressed to a given thickness. All mats were approximately one-inch thick so that the same system geometry could be maintained. For these measurements, flow rates were such that deformation did occur in the fiber mat. Thus, only one series of pressure drop-flow rate measurements could be taken because mat deformation is not fully recoverable.

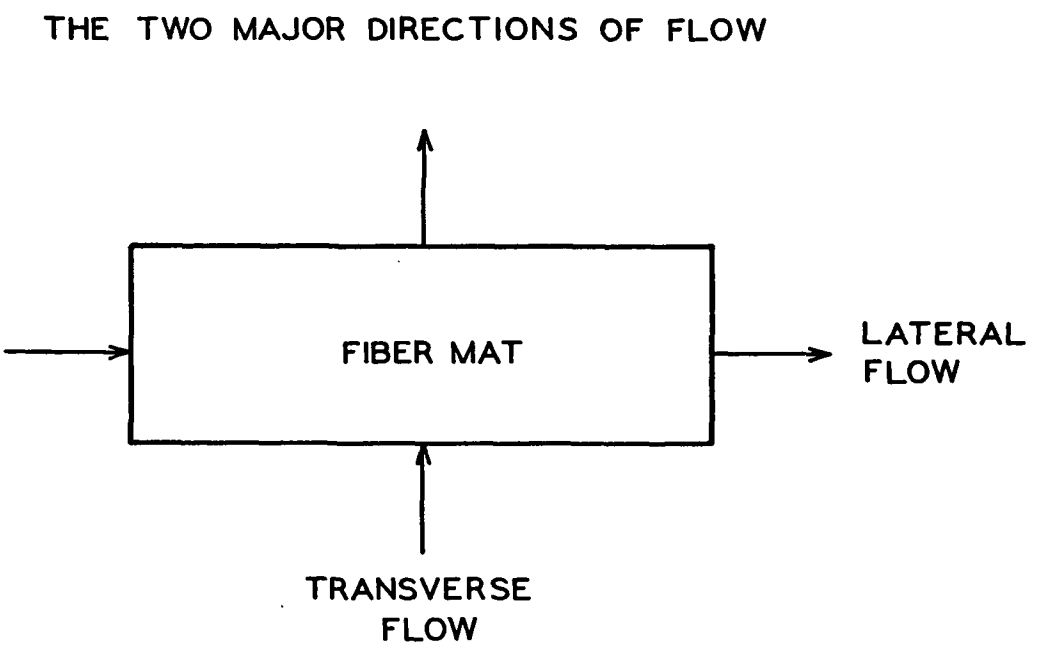

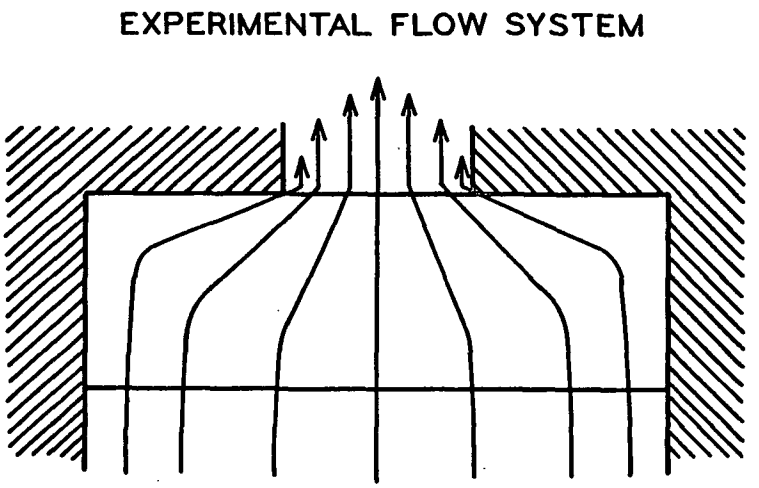

Figure 6. Two-Dimensional Flow

RESULTS AND DISCUSSION

As indicated earlier, to characterize two-dimensional flow through a deformable porous medium, several fiber and fiber mat properties must be known. These include the specific surface and specific volume of the fibers and the deformability and permeability characteristics of the fiber mat. Once these individual properties are known, they may be combined with the mathematical solution discussed earlier to describe the entire system.

BASIC PROPERTIES

FIBER PROPERTIES

As was discussed earlier, the determination of the basic fiber properties of specific surface and specific volume is a relatively simple task for inert cylindrical fibers. The microscopic determination of the average fiber diameter permits calculation of the specific surface area. Detailed results of this procedure for the nylon fibers used in this study are presented in Appendix V. Because the nylon fibers were solid, the fiber specific volume is just the inverse of the fiber density. This density, along with a few other fiber properties may be found in Appendix V.

MAT COMPRESSIBILITY

The two-dimensional flow system consists of a confined mat subject to fluid flow. Under these conditions the overall mass of the mat must remain constant (thus average mat concentration does not change), but there will be a redistribution of the mass within the mat because of fluid flow. An equation to approximate this redistribution was developed and is presented below. (See Appendix I for the details of this development.)

$$c = (1-\varepsilon)\rho_f = M\,(P_I - \Delta P_t/B + P_{i,j})^N \qquad (21)$$

where

$$B = \left[\frac{1}{(1 - N/2)^2}\right]^{1/N}.$$

This equation predicts the mat concentration c at any point in the mat as a function of the initial mechanical compressive pressure P_I, the total pressure drop across the mat ΔP_t at a fixed x, and the pressure $P_{i,j}$ at the particular point in the mat. In order to use this equation, the compressibility constants (M and N) of the fiber mat must be known. These were determined experimentally and these experimental compressibility data are shown in Fig. 7.

MAT PERMEABILITY

Fiber mat permeability data were correlated with the Davies-Ingmanson expression. This has the form

$$k = \frac{k_1 \varepsilon^3}{(1-\varepsilon)^{1/2}} \cdot [1 + k_2(1-\varepsilon)^3] \qquad (4)$$

where k is the Kozeny factor in the Kozeny-Carman equation. Ingmanson was able to fit a large amount of transverse permeability data on synthetic cylindrical fibers with this equation using the constants $k_1 = 3.5$ and $k_2 = 57$. The transverse permeability data from this study also agreed well with this correlation, as seen in Fig. 8. The lateral permeability data from this study could also be fitted with this equation using the constants $k_1 = 2.8$ and $k_2 = 50$. These data are also shown in Fig. 8. In this figure, the solid lines represent the mathematical correlation, while the experimental data are indicated as discrete points.

The generally good agreement of the transverse data from this study with Ingmanson's earlier data indicates that the square design of the filtration tube caused no particular

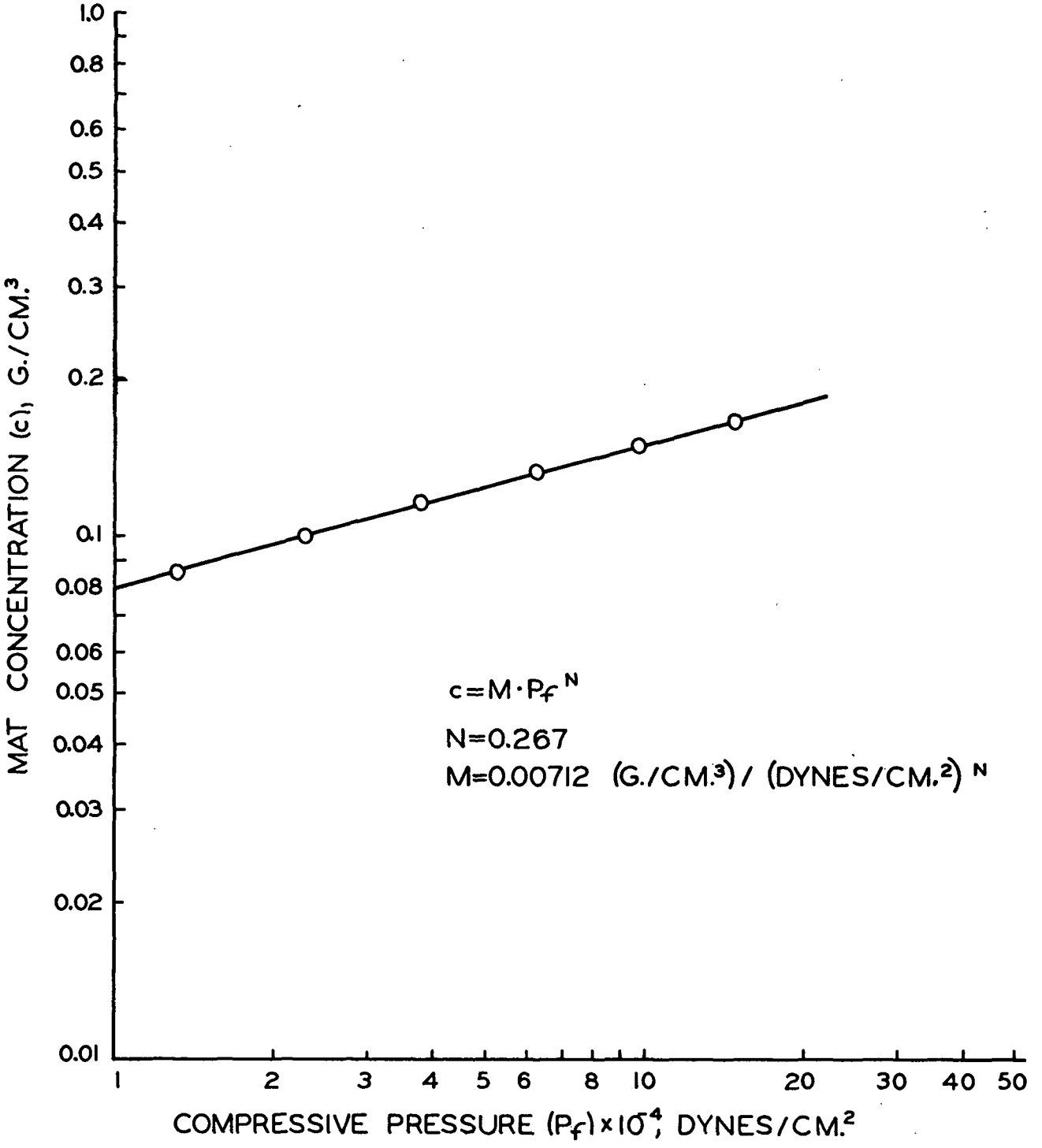

Figure 7. Fiber Mat Compressibility

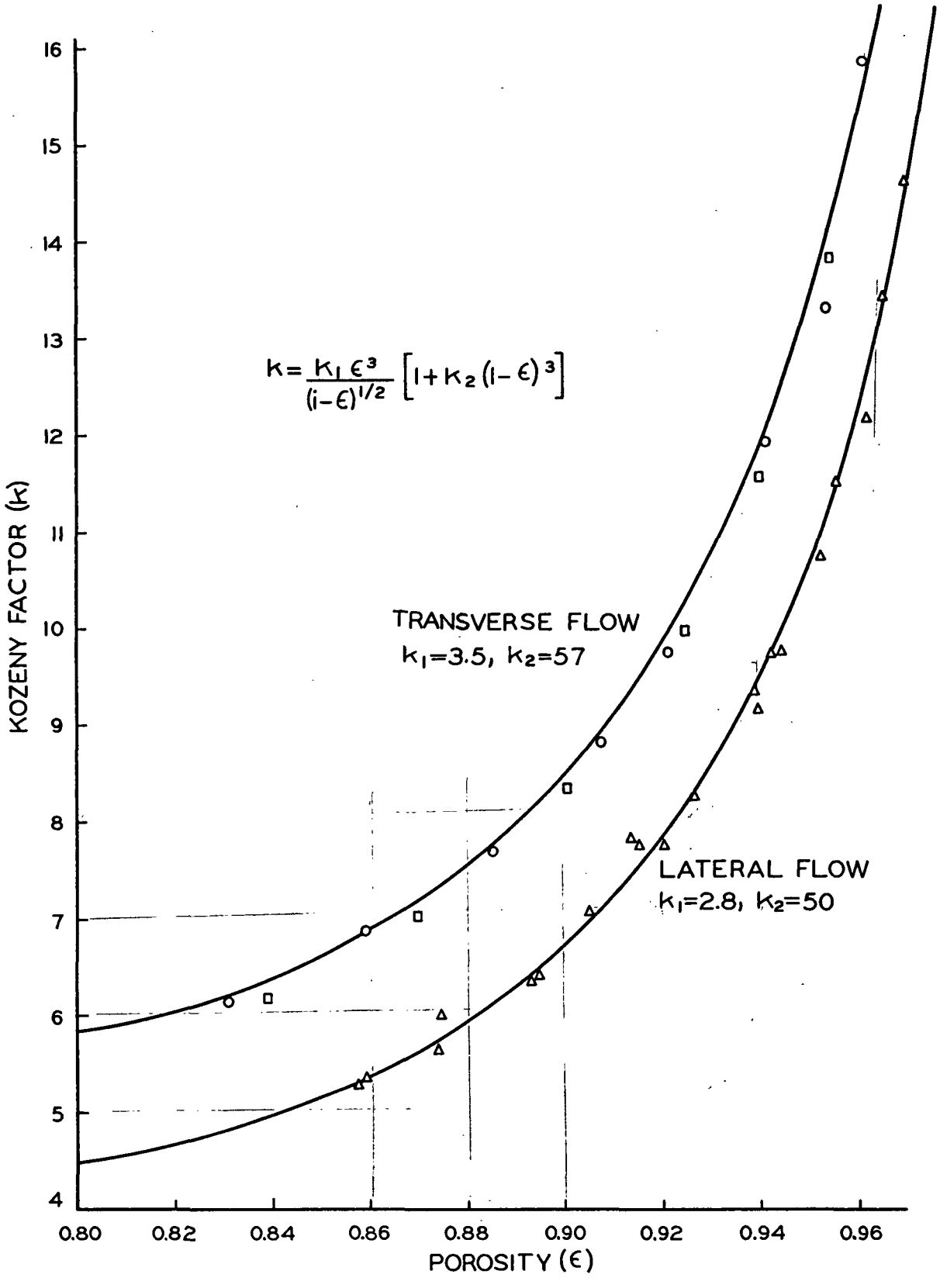

Figure 8. Kozeny Factor Correlations

problems. There had been some fear that this design would cause formation problems, but except for a slight build-up of fibers in the corners, these fears were groundless. Even this orientation problem at the corners seemed to have little effect on the overall results.

The results shown in Fig. 8 indicate that the Kozeny factor for lateral flow is considerably smaller than that for transverse flow for all values of the porosity. This is due to the different orientation of the fibers for lateral and transverse flow. Mat formation is such that essentially all fibers are oriented with their axes in the x-y plane. Thus, in the transverse direction, almost all flow is perpendicular to the fiber axes. However, in the lateral direction, the fiber axes are oriented both perpendicular and parallel to flow (and also all the possible angles in between the two extremes). Happel's drag theory (8) predicts that the Kozeny factor for flow parallel to cylinders should be less than that for flow perpendicular to cylinders. Therefore, the experimental data follow the predicted trends.

Fowler and Hertel's studies (43) on the effect of fiber orientation may also be used to check the experimental results. Their studies show that at the lower porosities ($\varepsilon < 0.8$) for flow perpendicular to the fiber axes, the Kozeny factor should be approximately 6.0. At low porosities the transverse data of this study approach a value of about 5.5. This value seems very reasonable when the probability that all fibers are not oriented strictly perpendicular to the direction of macroscopic flow is taken into account. For completely random orientation in three dimensions, Fowler and Hertel predict a Kozeny factor of 4.5. However, in the case of lateral flow through fiber beds, there is only random orientation in the two dimensions of the horizontal plane. Thus, theoretically k would be expected to have a value somewhat below 4.5, but greater than the value of 3.0 predicted for flow parallel to the fiber axes. The extrapolation of the lateral permeability data to lower porosities

yields a Kozeny factor of about 4.0, which seems well in line with the above theoretical considerations.

The Kozeny factor data can be easily translated into transverse and lateral permeabilities by substituting the Davies-Ingmanson correlation into the Kozeny-Carman equation. These results are presented in Fig. 9. (It should be noted that the permeability scale in this figure is logarithmic.) This plot shows clearly that the lateral permeability is greater than the transverse permeability. Thus, there is less resistance to flow in the lateral direction than in the transverse direction. The magnitude of this difference varies slightly with porosity, but generally the lateral permeability is 25-30% greater than the transverse permeability. This is certainly a significant difference and indicates a rather large difference in flow properties in the two directions.

TWO-DIMENSIONAL FLOW

The basic fiber and fiber mat properties, as reported in the preceding section, were the only experimental properties needed to predict theoretically the two-dimensional flow behavior in an anisotropic, deformable medium. Thus, once these were measured, it was possible to begin measurements on the two-dimensional, deformable flow system. However, before this work was started, it was considered desirable to obtain an independent check on the two-dimensional flow system.

ISOTROPIC MEDIA

This independent check was available for the case of two-dimensional flow through an isotropic medium. Engelund (35) had obtained an approximate solution for the case of two-dimensional flow in an isotropic medium for the same boundary conditions of this study. For laminar flow, he obtained the following equation for the overall pressure drop:

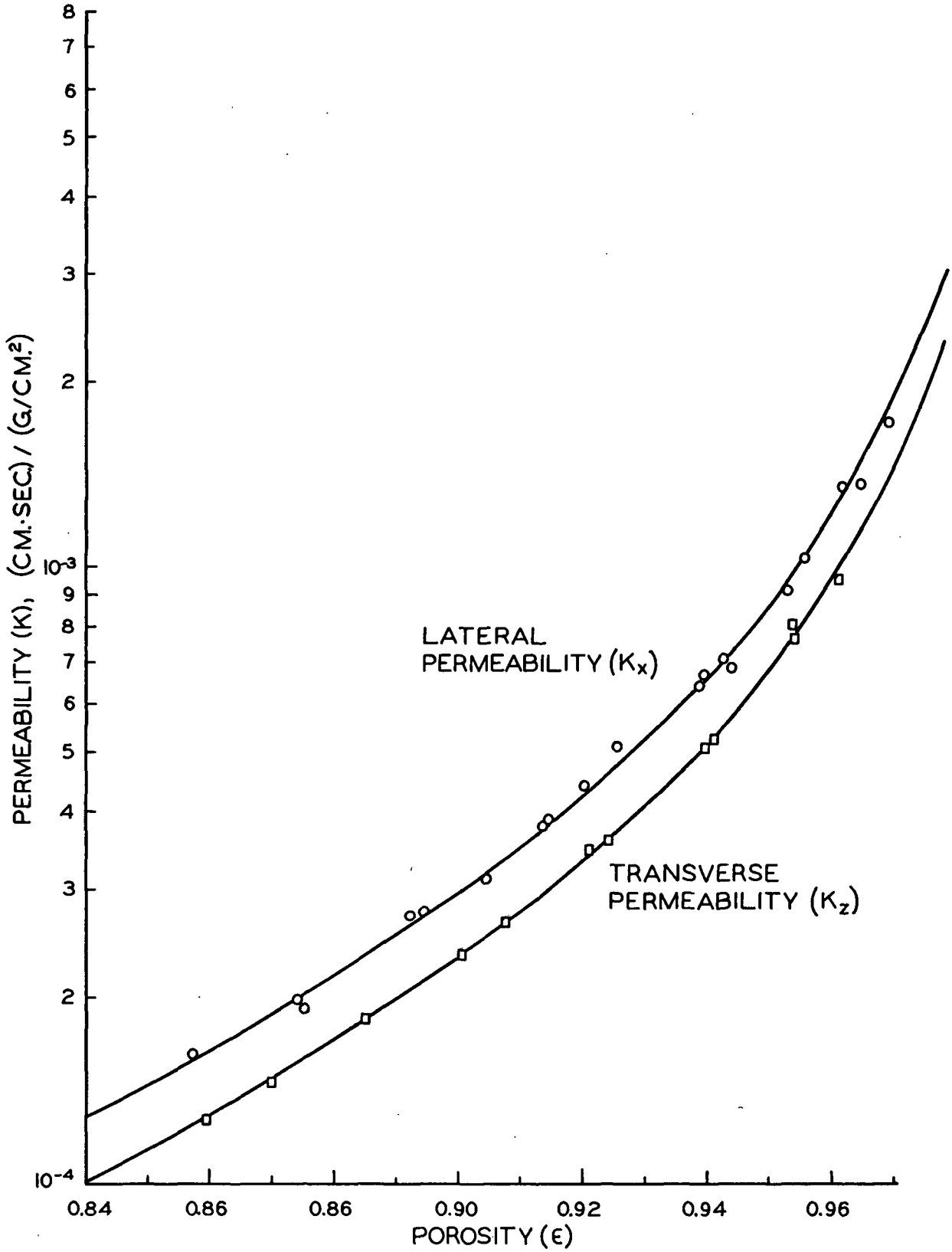

Figure 9. Permeability Coefficients

$$\Delta P = \frac{1}{K_o}\left(\frac{L}{A} + \frac{1}{\pi \ell} \ln \frac{2w}{\pi \delta}\right) \cdot Q \qquad (22)$$

where

ΔP = overall pressure drop

Q = volumetric flow rate

K_o = true permeability of the isotropic medium

L = thickness of the bed

A = cross-sectional area

ℓ = length of slot

w = width of the bed ($A = w \cdot \ell$)

δ = width of the slot

This equation states that the overall pressure drop is due to the additive effects of the pressure loss because of flow through the material and the pressure loss due to flow convergence through the slot. In deriving this equation, Engelund assumed that (1) the thickness of the porous medium was very large (semi-infinite) in comparison to its other dimensions, and (2) the width of the slot was small when compared to the width of the porous medium ($w/\delta > 3$).

Experimental data on two-dimensional flow through an isotropic bed of glass beads were obtained. Experimental conditions were such that Engelund's basic assumptions applied. Behavior of this same system was then predicted theoretically with the computer. The results of these three independent studies are presented in Table II. The apparent permeability K_{App} is introduced in Table II as a convenient method of correlating the overall two-dimensional flow data. Under a given set of conditions, the ratio of the flow rate to the pressure drop is a constant for flow through non-deformable media. Thus, the apparent permeability may be obtained by applying Darcy's law to the overall system:

$$K_{App} = (Q/\Delta P) \cdot (L/A). \qquad (23)$$

It should be emphasized here that this apparent permeability is in no way a true permeability. It was arbitrarily introduced here to reflect changes in the resistance of the overall system. Any changes in the actual permeable nature of the porous medium will show up as changes in $\underline{K}_{App}$. In addition, changes in system geometry which cause changes in the overall resistance of the system will be detected as changes in $\underline{K}_{App}$.

TABLE II

PERMEABILITY RESULTS FOR ISOTROPIC MEDIA

Slot Width, inches	$\underline{K}_{App} \times 10^4$, (cm.·sec.)/(g./cm.^{2})		
	Engelund	Computer	Experimental
1	3.48	3.51	3.52
1/2	3.25	3.32	3.31
1/4	2.97	3.16	3.10

This is by no means the only way to account for changes in the system. Changes in the system geometry do not actually change the permeability of the medium, but rather these changes affect the mean flow rate within the medium. Thus, some authors have preferred to attach a factor to $\underline{Q}$ to account for this change. However, since in this study changes were occurring in both the overall system and also within the porous medium itself, it was decided the use of $\underline{K}_{App}$ could best reflect all of these changes. (See Appendix IV for a further discussion of $\underline{K}_{App}$.)

Comparing the values of $\underline{K}_{App}$ for the three studies on two-dimensional flow through isotropic media reveals general agreement. The computer predictions appear to represent the experimental data somewhat better than Engelund's approximation. Engelund's predictions are generally several percent low. This discrepancy arises because Engelund's assumption of a very thick bed was not fully met. As the bed thickness is reduced further, Engelund's prediction would be expected to be less and less accurate.

Because of the general agreement of the experimental and computer results with Engelund's theory, it was believed safe to proceed with the two-dimensional studies on deformable media. It appeared that the experimental system was producing the desired flow patterns and the mathematical model was adequately describing these experimental results.

ANISOTROPIC, DEFORMABLE MEDIA

Experimental data for two-dimensional flow through anisotropic deformable media were obtained by pumping water through a confined fiber mat. The mat was anisotropic because of its differing permeabilities in the transverse and lateral directions. Although confined so that it had a constant mass (and thus constant average porosity), the mat was deformable. The drag forces due to fluid flow were large enough so that changes in the porosity distribution within the mat could occur.

These experimental results were compared with the pressure drop-flow rate behavior predicted by the numerical solution of the flow equation. This comparison is shown in Fig. 10, 11, and 12. In these figures, the experimental data are shown as individual data points, while the theoretical predictions are the solid lines. The experimental data were obtained using three different slot widths at the indicated average mat porosities. The theoretical curves were obtained by integrating the pressure distributions and have been corrected for truncation error. This truncation error occurred because a rather coarse iteration mesh was used. This was necessary to reduce to a manageable level the relatively long computation times required to obtain a pressure distribution. To correct for this truncation error, the pressure distributions for a limited number of experimental conditions were solved using a smaller mesh spacing. Using values obtained at these two different mesh spacings, an estimate of the truncation error could be obtained. A detailed discussion of errors, along with the procedure for estimating the magnitude of the truncation error is presented in Appendix I.

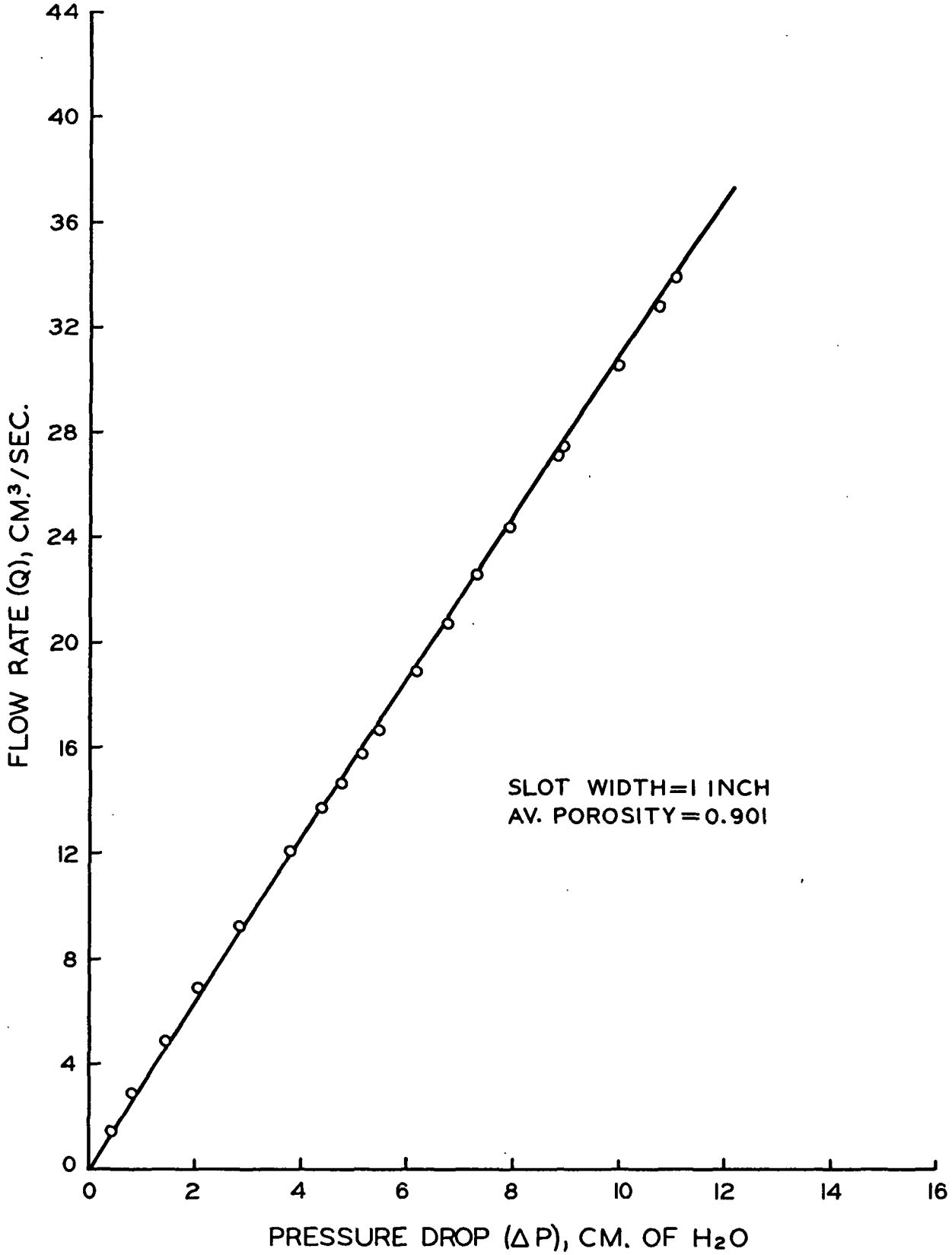

Figure 10. Two-Dimensional Flow Through a Deformable Medium

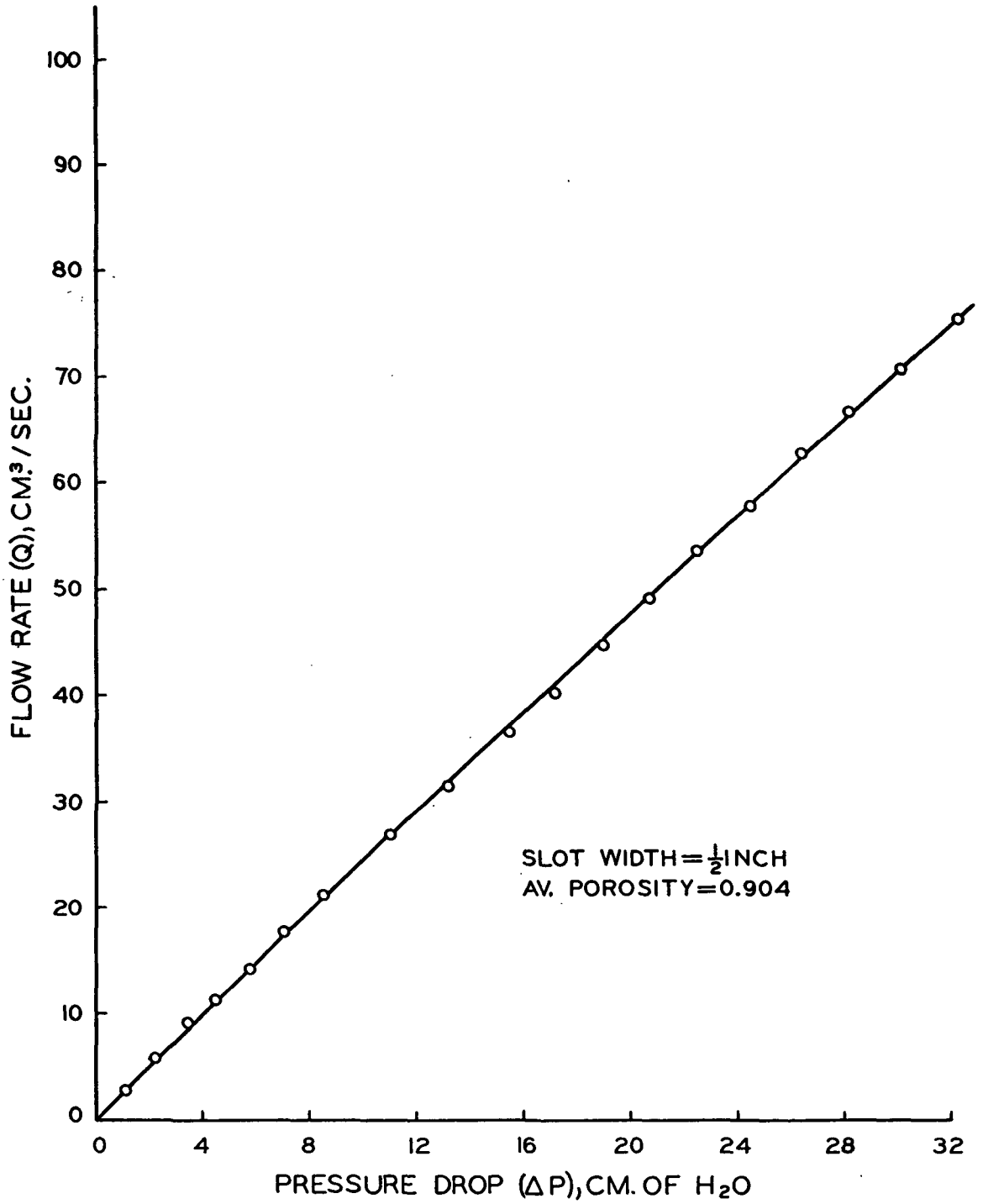

Figure 11. Two-Dimensional Flow Through a Deformable Medium

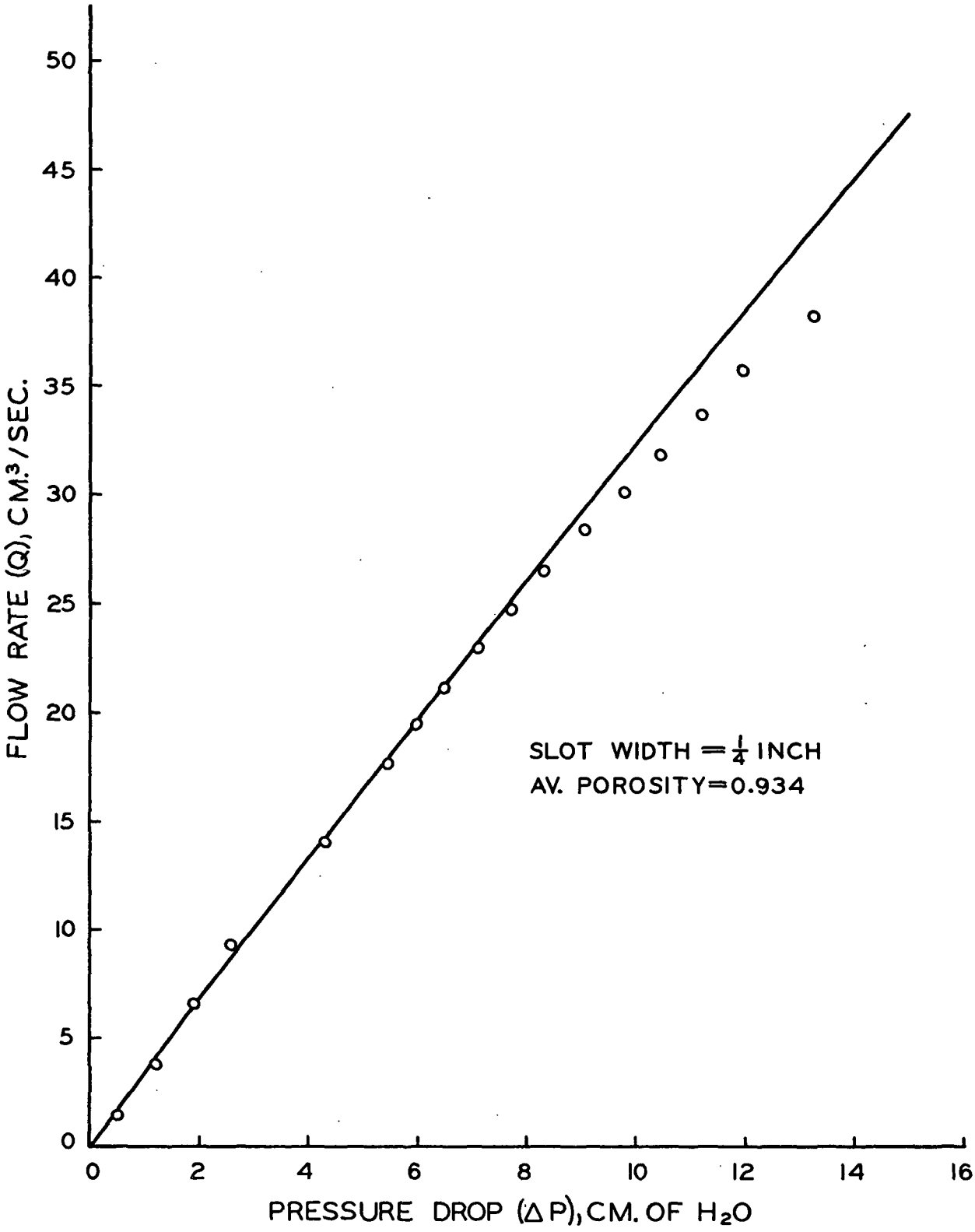

Figure 12. Two-Dimensional Flow Through Deformable Media

The experimental data in Fig. 10 and 11 show excellent agreement with the theoretical predictions. This would indicate that the assumptions made in developing the theory were probably valid, at least under the experimental conditions present in these two cases. The experimental results shown in Fig. 12, however, deviate considerably from the theoretical prediction at the higher flow rates. This behavior was not totally unexpected. These data represent the extreme case of a very small slot where the assumptions used in developing the theoretical equations were most likely to break down. For example, in deriving the two-dimensional flow equation, the terms containing the cross-permeabilities $\underline{\underline{K}}_{xz}$ and $\underline{\underline{K}}_{zx}$ were neglected. It was assumed that while these permeabilities were not zero, they were probably quite small. However, even though these permeabilities were small, they were multiplied by the pressure gradients, which were rather large near the slot. Thus, for this extreme case, it might be necessary to consider these terms. Another simplification which could have a major effect in this case was the use of an approximate one-dimensional deformability function. The omission of lateral compression was probably most serious in this case where the pressure gradients in the lateral direction were quite high near the slot. Other assumptions which could have caused the deviation observed in Fig. 12 include neglecting wall drag and assuming that only viscous losses were occurring. Neglecting wall drag probably couldn't lead to serious errors in this system, but it could contribute to the observed disagreement between the theoretical and experimental data. The use of Darcy's law in developing the flow equations assumes that only viscous losses were occurring. However, the flow rates near the slot were approaching the range in which inertial losses begin to show up. These additional inertial losses could also account for the divergence seen in Fig. 12. However similar flow rates were present near the slot for the system of Fig. 11. Since these experimental data do not deviate from the theoretical prediction, the effect of inertial losses can probably be discounted.

Experimental data of the type shown in Fig. 10, 11, and 12 were obtained at several different porosities for each of the three slot widths. It was thought desirable to convert these data into a form in which all data for a particular system could be compared at the same time. A study of the theoretical predictions at several different porosities revealed that if the flow rates were adjusted by dividing by the apparent permeability and the maximum pressure drop and these values were compared at the same relative pressures, then all the data for a particular system followed one theoretical curve. This procedure essentially places all the flow rate data on the same porosity basis and compares it after similar relative changes in the porosity distribution. A detailed justification of this procedure is presented in Appendix III.

Using this procedure to put all the pressure drop-flow rate data for a given geometrical system on the same basis, the results in Fig. 13, 14, and 15 are obtained. In these plots, the experimental data are again plotted as discrete points and the theoretical predictions as solid lines. As in the previous figures, the agreement between experiment and theory is fairly good. Because of the large number of runs, there is some scatter in the data. The divergence of the theoretical predictions and the experimental data for the case of the smallest slot width is again observed in Fig. 15.

Aside from the disagreement noted in the one case, the results of theory and experiment agree fairly well. Much of the scatter in the data can be attributed directly to the experimental technique. Slight fluctuations in flow rate and pressure drop could have caused much of the scatter in the data within a single run. Errors in the measurement of mat thickness and weight could have caused differences between runs. Another possible factor causing differences between runs was the difficulty in obtaining exactly the same formation from run to run. In light of the

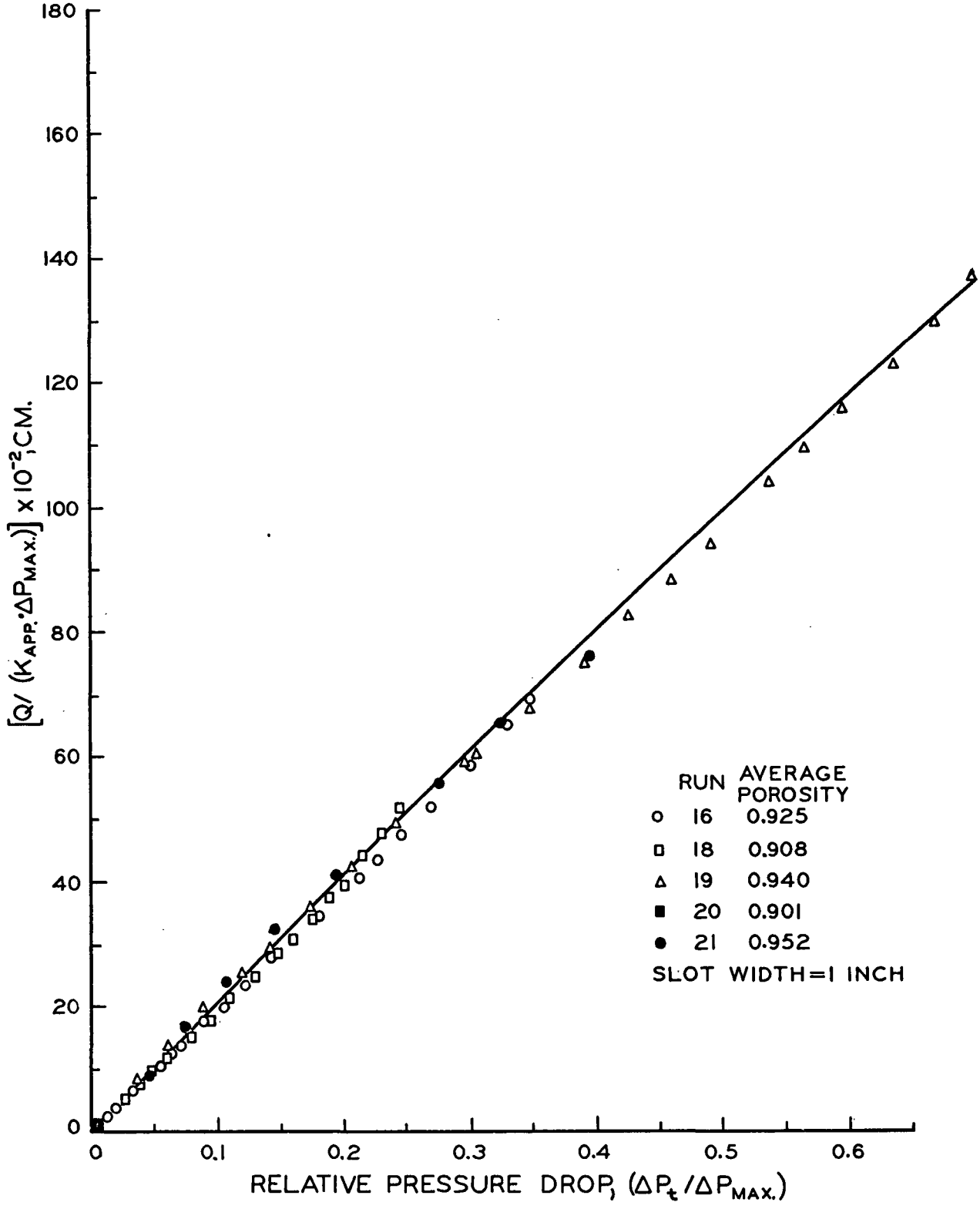

Figure 13. Two-Dimensional Flow Through Deformable Porous Media

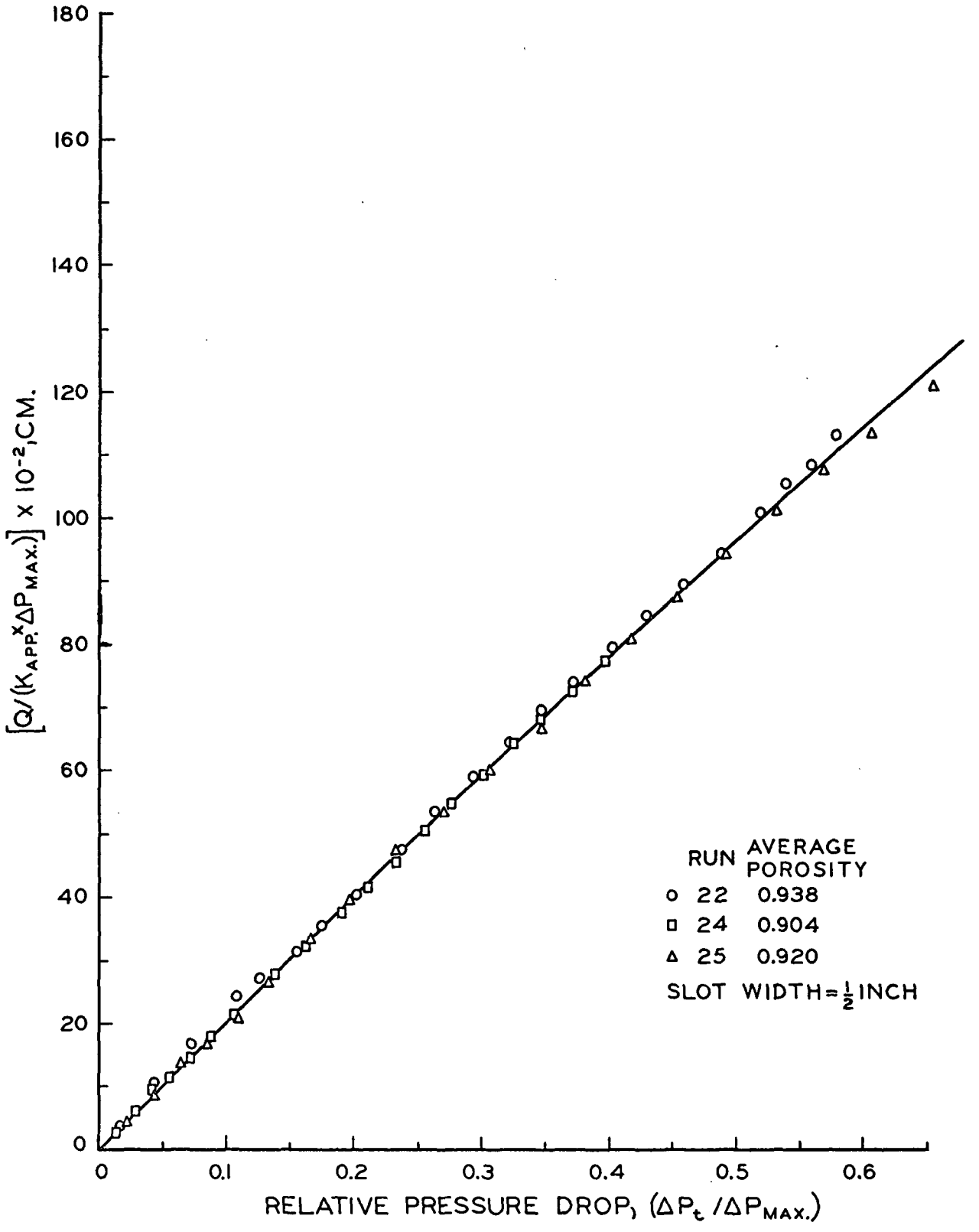

Figure 14. Two-Dimensional Flow Through Deformable Porous Media

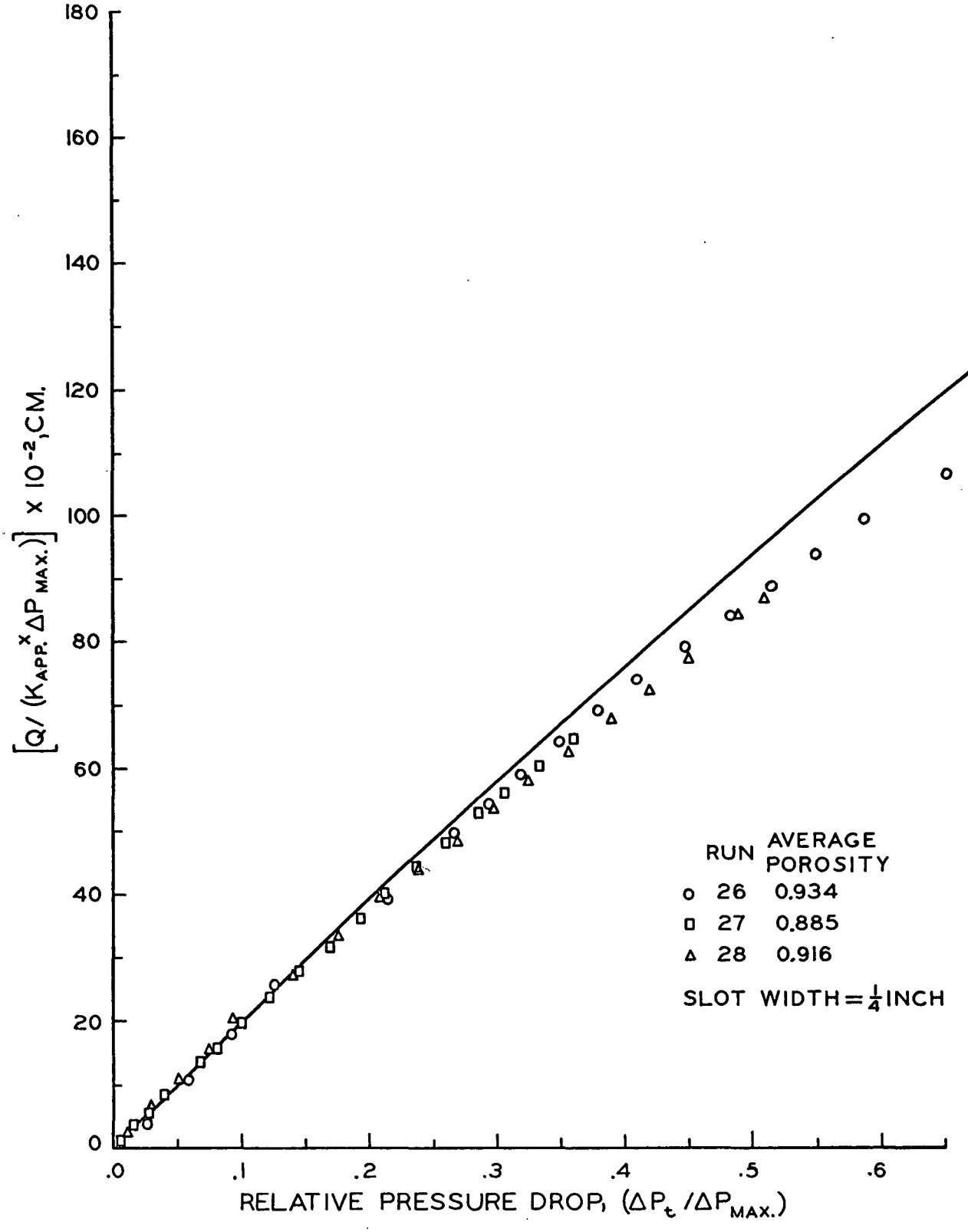

Figure 15. Two-Dimensional Flow Through Deformable Porous Media

possible influence of all of these experimental errors, the agreement of the experimental data and the theoretical curves appears quite acceptable.

NUMERICAL RESULTS

Obtaining agreement between the theoretical predictions and experimental data for two-dimensional flow through a deformable medium completed the major objective of this study. However, the computer is a valuable tool and much additional information can be obtained from the numerical solution of the two-dimensional flow equations. Thus, the numerical solution was used to estimate the relative importance of changes in the geometry of the system, and the porosity, deformability, and degree of anisotropy of the porous medium.

INFLUENCE OF MAT THICKNESS

For one-dimensional flow through a nondeformable medium, permeability is independent of the thickness of the material. However, for two-dimensional flow, the apparent permeability is a function of the thickness. Changing the thickness will alter the flow lines within the material and thus change the overall flow properties of the system. Perhaps this effect can be brought out more clearly by referring to Fig. 16. Each block in this figure contains a pressure distribution produced by the data mapping program. Only one-half of the porous medium is shown and each equal pressure line represents a drop of one-tenth of the total pressure across the mat. In these plots, only mat thickness has been changed, with all the other conditions being held constant. Thicknesses of 3/8, 3/4, and 1-1/4 inches are shown.

Even for these relatively small changes in thickness, marked differences can be seen in the pressure distributions (and thus the flow patterns) within the mats. For the thin mat, the great majority of the pressure drop is occurring in that section of the mat directly above the slot. Thus, there is little flow near the sides of the

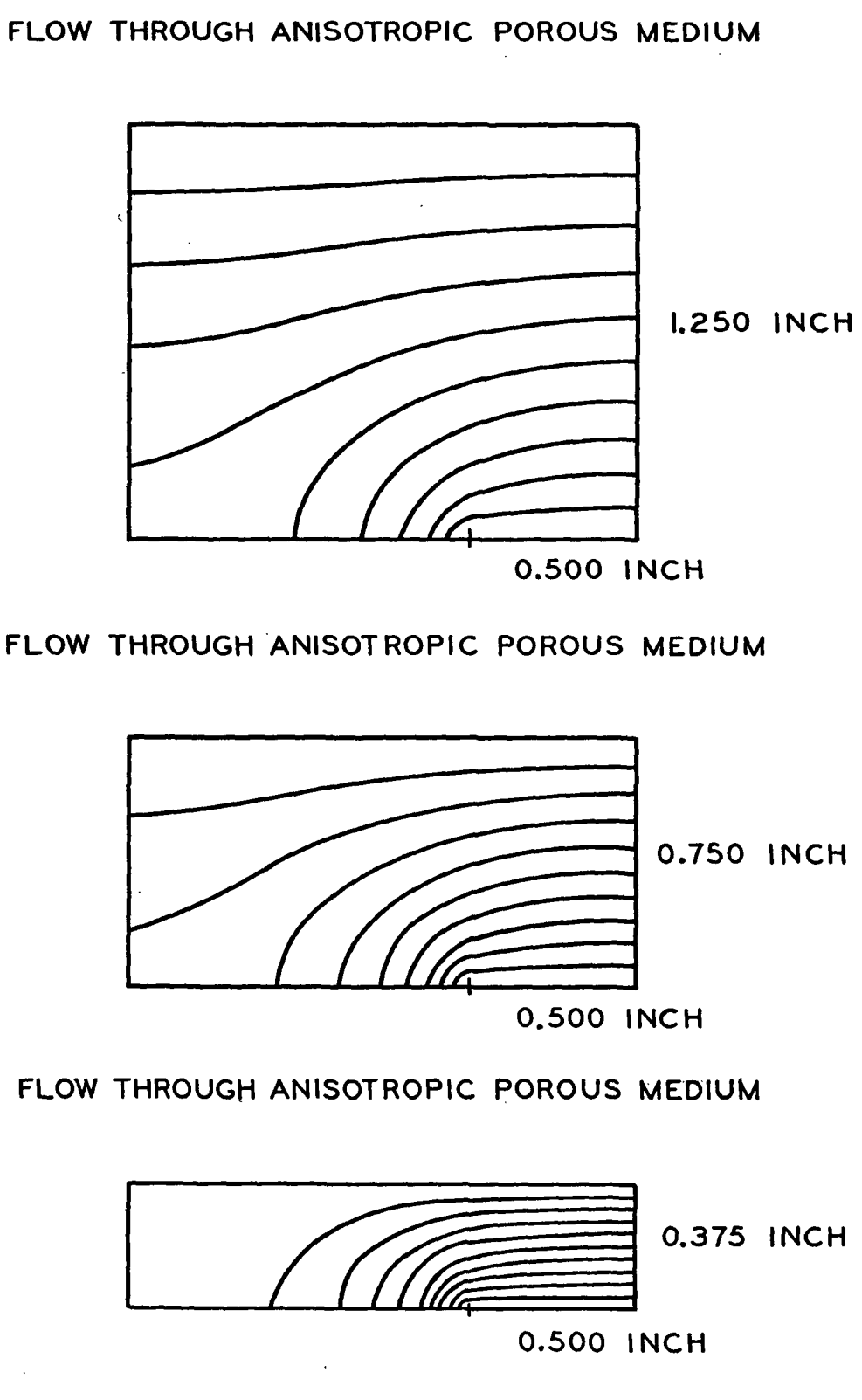

Figure 16. Dependence of the Pressure Distribution on Mat Thickness

mat. As the mat thickness increases, the contribution of the pressure drop near the slot to the total becomes smaller. Also the fluid tends to travel in relatively straight streamlines down through the mat until it gets fairly close to the slot.

It is interesting to plot the apparent permeability (determined from the overall flow rate, pressure drop, and cross-sectional area) versus the mat thickness. Such a plot is shown in Fig. 17. Of special interest is the value of $\underline{K}_{App}$ when extrapolated to zero mat thickness. It is found that this value equals the actual transverse permeability divided by the ratio of the total cross-sectional area to the slot cross-sectional area. Thus, for very thin mats, the flow appears to be one-dimensional and confined to the area right above the slot. The effective cross-sectional area available for permeation is thus reduced to the area of the slot.

The value of $\underline{K}_{App}$ at high mat thicknesses can also be predicted. The plots in Fig. 17 appear to level off at higher thicknesses. If they were carried out far enough, they should asymptotically approach the value of the actual transverse permeability. This behavior is due to the fact that as the thickness becomes larger, the relative contribution to the total pressure drop of the pressure drop around the slot becomes smaller. Indeed, it was found experimentally that at a thickness of 8.5 inches, the apparent permeability and the true transverse permeability were almost equal.

INFLUENCE OF SLOT WIDTH

The contour mapping plots of Fig. 18 show the influence of the slot width on the pressure distributions. In these plots, only the slot widths were changed, all other conditions being held constant. These figures indicate that as the slot width is decreased, an increasing percentage of the total pressure drop occurs near the slot. Thus, as slot width is decreased, the apparent permeability should also decrease.

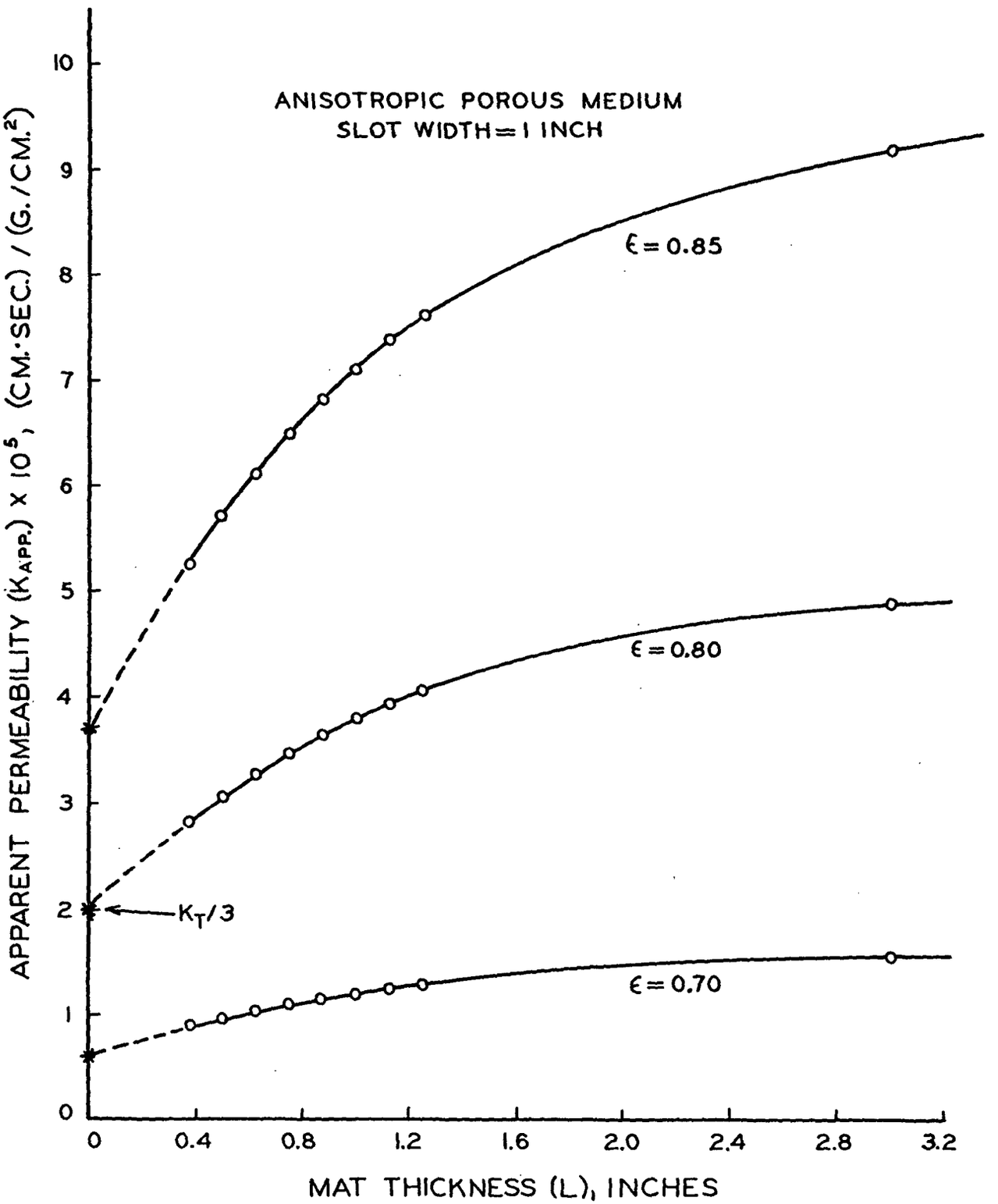

Figure 17. Variation of Apparent Permeability with Mat Thickness

This trend is pointed out in Fig. 19b. When no slot is present, the apparent permeability is equal to the true transverse permeability. However, as soon as an obstruction to flow is introduced into the porous medium, the apparent permeability decreases. This decrease in apparent permeability is caused by the convergence of flow through the slot causing higher fluid velocities within the mat near the slot. This results in a higher overall pressure drop at the same volumetric flow rate and thus decreased apparent permeability.

One practical aspect of this fact can be found in the studies of Perry (44) on the flow resistance of composite porous structures. He found that the presence of the wire caused a change in the flow lines within the mat above the wire from that found if the wire were absent. From his model studies, he estimated that 90% of the so-called mat-wire interaction was due to this convergence of the streamlines within the mat immediately above the wire. Also, as the thickness of the mat increased, this interaction became less and less important.

DEGREE OF ANISOTROPY

As was shown earlier, a fiber mat is definitely anisotropic, with different permeabilities in the transverse and lateral directions. However, the question remains as to how important this effect is and how much error would be involved in assuming the medium to be isotropic. The magnitude of error in this assumption depends on the relative amounts of transverse and lateral flow. If, for example, the medium was assumed isotropic with a permeability equal to the normal transverse value; then for the extreme case of complete lateral flow, an error of 25-30% would be involved. But for most two-dimensional flow cases, there is a combination of transverse and lateral flow and an error of lesser magnitude would be expected. Figure 19a shows one such flow situation and an average error of about 7-8% is

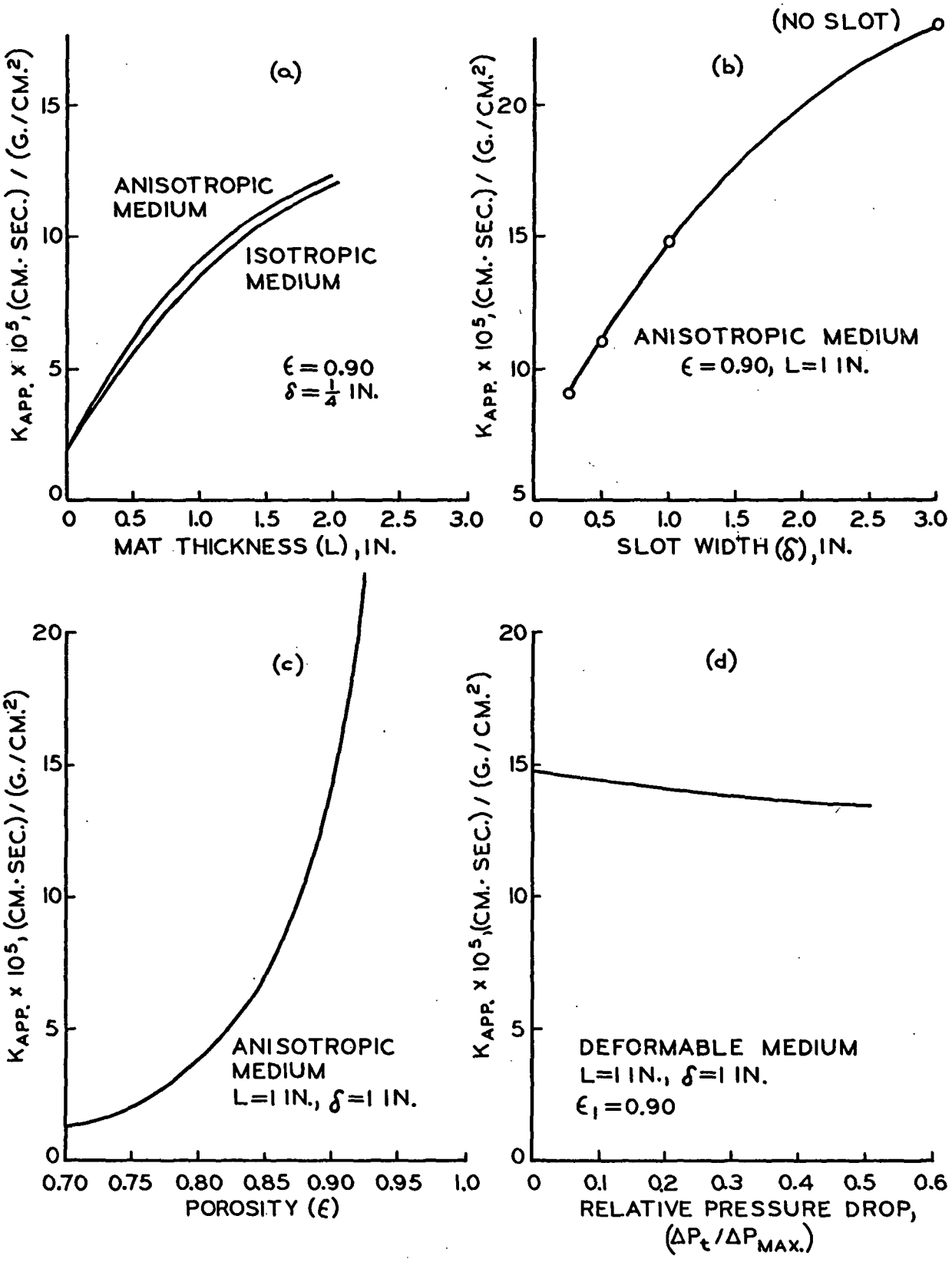

Figure 19. Variation of Apparent Permeability with Mat Properties

involved. Thus, in general, this assumption is not extremely critical, but would depend on the relative amounts of transverse and lateral flow in the particular system.

DEFORMABILITY

Drag forces, caused by the flow of a fluid through a deformable medium, have two major effects on the nature of the medium. First, they cause a change in the average porosity of the medium and second, they cause a change in the porosity distribution within the medium. Both of these effects result in changes in the permeability properties of the porous medium. Figures 19c and 19d give an idea of the relative importance of these two changes. First, the general consolidation of the mat due to drag forces results in a decrease in the average porosity of the mat. As seen in Fig. 19c, relatively small changes in the porosity result in large changes in the permeability. At the same time there is a change in the average porosity, there is also a change in the porosity distribution within the porous medium. This effect is shown in Fig. 19d. This represents a mat held at a constant average porosity. Increases in the pressure drop due to fluid flow change only the porosity distribution within the mat. When there is no flow, the porosity of the mat is uniform throughout. As the flow rate (and thus the pressure drop) is increased, a distribution of porosities results, with a maximum porosity at the entrance face of the mat and a minimum porosity at the exit face. This change in the porosity distribution causes a decrease in the apparent permeability. However, for the range covered here, this represents only an 8-9% decrease in overall permeability. Thus, the major change in apparent permeability due to mat deformation is caused by the change in average porosity, while changes in porosity distribution cause relatively minor effects.

CONCLUSIONS

The experimental results of this study have conclusively shown that there are significant differences in the flow properties of fiber mats in the two major directions of flow. The lateral permeability was found to be 25-30% greater than the permeability in the transverse direction. This difference was caused by the greater number of fibers oriented parallel to the direction of lateral flow.

This study also showed that it was possible to predict the two-dimensional flow behavior of a porous medium by a simple numerical solution of the two-dimensional flow equations. This was confirmed by the work on isotropic porous media where the numerical results agreed well with the experimental measurements and also with the approximate predictions of Engelund. Agreement of within 1-2% was also obtained between the numerical and experimental data on two-dimensional flow through deformable porous media. Only in the extreme case of the smallest slot width was there significant divergence of the theoretical and experimental results. This difference was probably due to several simplifying assumptions made in developing the theory.

In addition to predicting the flow behavior of the experimental system, the computer solutions of the flow equation yielded qualitative information on the relative importance of various factors affecting flow. Changes in system geometry (mat thickness and slot width) were found to be of prime importance. These changes caused major changes in the pressure distributions within the porous medium and thus major changes in the overall pressure drop-flow rate measurements. Mat compressibility was also found to be very important. The major effect of compressive forces was found to be the change in average porosity, resulting in greatly decreased permeabilities. Of less importance were changes in the porosity distribution within the porous medium, which also resulted in decreased overall permeabilities. Finally, the

anisotropic nature of the medium affected the overall permeability. This effect was found to be dependent on the relative amounts of transverse and lateral flow in the system.

Thus, this study should provide an increased understanding of flow through fibrous materials. It has pointed out the complex nature of these materials and how changes in the system result in changes in the overall flow properties in two-dimensional flow.

SUGGESTIONS FOR FURTHER WORK

Even though this study was greatly simplified in several ways, many useful conclusions resulted. However, a study in greater depth could yield additional useful information.

Perhaps the greatest simplifications employed in this study involved mat compressibility. These were used because of limitations of both the experimental system and the mathematical model. It is experimentally very difficult to measure mat compression in the lateral direction. Interactions between lateral and transverse compression would be even more difficult to determine. However if estimates of these quantities could be obtained, they could be included in a more complete compressibility model. With the addition of the more sophisticated computing facilities at the Institute, it might be possible to consider this more complex problem.

This study considered only a confined fiber mat maintained at the same average mat concentration. Thus, fluid drag forces resulted in only changes in the porosity distribution. To more closely approximate actual situations, an unconfined mat might be considered, where changes in both average porosity and porosity distribution are occurring. This would involve changing mat thicknesses and probably also changes in the curvature of the mat surface.

Perhaps the other most important limitation of this study was the consideration of only viscous dissipation losses. This assumption allowed the use of Darcy's law. However, there are many practical cases where inertial losses are also important, if not controlling. Thus, an extension of the study to higher flow rates and the use of the Forchheimer equation might be valuable. In conclusion, while much useful information has been obtained from this study, an extension to more fully account for mat compressibility and the introduction of inertial losses should provide increased understanding of flow through fibrous materials.

SYMBOLS AND NOMENCLATURE

a = viscous coefficient of Forchheimer equation

A = cross-sectional area, cm.^{2}

b = inertial coefficient of Forchheimer equation

c = fiber mat density or concentration, g./cm.^{3}

c_o = mat density at zero applied load, g./cm.^{3}

h = mesh spacing in iteration procedure, cm.

k = Kozeny factor in Kozeny-Carman equation

k_1, k_2 = constants in Ingmanson-Davies correlation

$k_{\parallel}$, $k_{\perp}$ = Kozeny factors for flow parallel and perpendicular to cylinders (Happel's theory)

K = permeability coefficient, (cm.-sec.)/(g./cm.^{2})

K_{App} = apparent permeability, (cm.-sec.)/(g./cm.^{2})

K_o = true permeability in Englünd's equation, (cm.-sec.)/(g./cm.^{2})

$K_{\parallel}$, $K_{\perp}$ = Happel's permeabilities for flow parallel and perpendicular to cylinders, (cm.-sec.)/(g./cm.^{2})

ℓ = length of slot in Engelund's equation, cm.

L = thickness of porous medium, cm.

m = total number of columns of mesh points in iteration procedure

M = compressibility constant

n = total number of rows of mesh points in iteration procedure

N = compressibility constant

P = hydrostatic pressure, cm. H_2O

P_f = compressive pressure on fibers, cm. H_2O

P_I = initial compacting pressure, cm. H_2O

$P_{i,j}$ = pressure at any point, i,j due to fluid flow, cm. H_2O

ΔP_{Max} = total pressure drop across fiber mat at which mat will lift away from the lower surface, cm. H_2O

ΔP_t = total pressure drop across fiber mat at a constant x, cm. H_2O

Q = volumetric flow rate, $cm.^3/sec.$

S_v = specific surface area of the fibers, $cm.^{-1}$

u_x = velocity component in the lateral direction, cm./sec.

u_z = velocity component in the transverse direction, cm./sec.

v = specific volume of the fibers, $cm.^3/g.$

w = width of bed in Engelund's equation, cm.

x = x-coordinate; lateral direction

y = y-coordinate

z = z-coordinate; transverse direction

δ = width of slot, cm.

ε = porosity

γ = Wilder's compressibility constant

μ = viscosity of fluid, g./(cm.-sec.)

π = 3.1416

ρ = density of the fluid, $g./cm.^3$

ρ_f = density of the fibers, $g./cm.^3$

ω = relaxation parameter in the iteration procedure

ω_{opt} = optimum relaxation parameter

exp = exponential function

ln = natural log

∇^2 = Laplacian operator

Subscripts

f = refers to fiber properties

I = refers to initial conditions

i = index in x-direction

$\underline{j}$ = index in $\underline{z}$-direction

$\underline{L}$ = refers to open face of the fiber mat

0 = refers to septum face of the fiber mat

$\underline{x}$ = refers to $\underline{x}$-direction

$\underline{y}$ = refers to $\underline{y}$-direction

$\underline{z}$ = refers to $\underline{z}$-direction

ACKNOWLEDGMENTS

Sincere thanks are due to Mr. Heribert Meyer, Chairman of my Advisory Committee, for his guidance and support from the conception of this study. The advice and encouragement of the other members of the committee, Dr. Thomas Grace and Dr. Richard Nelson, are also greatly appreciated.

The entire Institute staff has been most helpful. My thanks go to the faculty for giving me the necessary background to undertake such a study. Special thanks are due Paul Van Rossum and Marvin Filz for their help in the design and construction of the experimental apparatus. Jack Hankey's microscopic determination of average fiber diameters was a great help. The guidance of John Bachhuber during the computer work was also appreciated. The continued help and advice of Bruce Andrews during the entire program was invaluable.

My fellow students also deserve credit. Their friendship and companionship have made my work much easier. To John Perry, sincere thanks for help with both the experimental system and the numerical calculations.

Last, but certainly not least, my wife Pat deserves a medal. My deepest thanks for help in the preparation of this manuscript and for putting up with me for the last two and one-half years.

LITERATURE CITED

1. Kozeny, J., Sitzber. Akad. Wiss. Wein, Math. naturw. Klasse, 136 (Abt. IIa): 271-306(1927).

2. Carman, P. C., Trans. Inst. Chem. Eng. (London) 15:150-66(1937).

3. Sullivan, R. R., and Hertel, K. L., J. Appl. Phys. 11, no. 12:761-5(Dec., 1940).

4. Sullivan, R. R., J. Appl. Phys. 12, no. 6:503-8(June, 1941).

5. Emersleben, O., Physik. Z. 26:601(1925).

6. Burke, S. P., and Plummer, W. B., J. Ind. Eng. Chem. 20:1200-4(1929).

7. Iberall, A. S., J. Res. Natl. Bur. Std. 45:398-406(1950).

8. Happel, J., A.I.Ch.E. Journal 5, no. 2:174-7(June, 1959).

9. Davies, C. N., Proc. Inst. Mech. Engrs. (London) 1B:185(1952).

10. Ingmanson, W. L., Andrews, B. D., and Johnson, R. C., Tappi 42, no. 10:840-9 (Oct., 1959).

11. Carroll, C. W. In The status of the sheet forming process. Appleton, Wis., The Institute of Paper Chemistry, 1965.

12. Campbell, W. B., Pulp Paper Mag. Can. 48, no. 3:103-9(1947).

13. Ingmanson, W. L., and Whitney, R. P., Tappi 37, no. 11:523-34(Nov., 1954).

14. Wilder, H. D., Tappi 43, no. 8:715-20(Aug., 1960).

15. Jones, R. L., Tappi 46, no. 1:20-8(Jan., 1963).

16. Elias, T. C. An investigation of the compression response of ideal unbonded fibrous structures by direct observation. Doctor's Dissertation. Appleton, Wis., The Institute of Paper Chemistry, 1965.

17. Han, S. T. In The status of the sheet forming process. Appleton, Wis., The Institute of Paper Chemistry, 1965.

18. Ingmanson, W. L., Chem. Eng. Progr. 49, no. 11:577-84(1953).

19. Ingmanson, W. L., Tappi 35, no. 10:439-48(Oct., 1952).

20. Whitney, R. P., Ingmanson, W. L., and Han, S. T., Tappi 38, no. 3:157-66 (March, 1955).

21. Grace, H. P., Chem. Eng. Progr. 49, no. 6:303-18(June, 1953); no. 7:367-77 (July, 1953); no. 8:427-42(Aug., 1953).

22. Hisey, R. W., Tappi 39, no. 10:690-6(Oct., 1956).

23. Hutto, F. B., Jr., Chem. Eng. Progr. 53, no. 7:328-32(July, 1957).

24. Tiller, F. M., A.I.Ch.E. Journal 4, no. 2:170-4(June, 1958).

25. Tiller, F. M., and Cooper, H., A.I.Ch.E. Journal 8, no. 4:445-9(Sept., 1962).

26. Shirato, M., Sambuichi, M., and Okamura, S., A.I.Ch.E. Journal 9, no. 5:599-605 (Sept., 1963).

27. Tiller, F. M., and Huang, C. J., Ind. Eng. Chem. 53, no. 7:529-37(July, 1961).

28. Ingmanson, W. L., Tappi 47, no. 12:742-50(Dec., 1964).

29. Meyer, H., Tappi 45, no. 4:296-310(April, 1962).

30. Ingmanson, W. L., and Andrews, B. D., Tappi 46, no. 3:150-5(March, 1963).

31. Nelson, R. W., Tappi 47, no. 12:752-64(Dec., 1964).

32. Muskat, M. The flow of homogeneous fluids through porous materials. New York, McGraw-Hill, 1937.

33. Scheidegger, A. E. The physics of flow through porous media. Revised ed. Toronto, University of Toronto Press, 1960.

34. Streeter, V. L. Fluid dynamics. New York, McGraw-Hill, 1948.

35. Engelund, F., Trans. Danish Acad. Tech. Sci. no. 3 (1953).

36. Kirkham, D., J. Appl. Phys. 21, no. 7:655-60(July, 1950).

37. Brenner, H., A.I.Ch.E. Journal 7, no. 4:666-71(Dec., 1961).

38. Johnson, W. E., and Hughes, R. V., Producers Monthly 13, no. 1:17-25(1948).

39. Biot, M. A., J. Appl. Phys. 12:155-64(Feb., 1941).

40. Biot, M. A., J. Appl. Phys. 26, no. 2:182-5(Feb., 1955).

41. Paria, G., Appl. Mech. Rev. 16, no. 6:421-3(June, 1963).

42. Perry, J. F. Private communications, 1968.

43. Fowler, J. L., and Hertel, K. L., J. Appl. Phys. 11, no. 7:496-502(July, 1940).

44. Perry, J. F. A study of the flow resistance of composite porous structures. Doctor's Dissertation. Appleton, Wis., The Institute of Paper Chemistry, 1968.

45. Lapidus, L. Digital computation for chemical engineers. New York, McGraw-Hill, 1962.

46. Douglas, J., Jr., and Peaceman, D. W., A.I.Ch.E. Journal 1, no. 4:505-12 (Dec., 1955).

47. The status of the sheet forming process. Appleton, Wis., The Institute of Paper Chemistry, 1965.

48. McCracken, D. D., and Dorn, W. S. Numerical methods and Fortran programming. New York, John Wiley and Sons, 1964.

APPENDIX I

FINITE DIFFERENCE SOLUTION OF THE TWO-DIMENSIONAL FLOW EQUATIONS

FORMULATION OF THE DIFFERENCE EQUATIONS

The flow equations presented earlier in the section on theoretical development are repeated again here. For two-dimensional flow through isotropic media:

$$\frac{\partial^2 P}{\partial x^2} + \frac{\partial^2 P}{\partial z^2} = 0. \tag{19}$$

For flow through anisotropic, nondeformable media:

$$K_{xx} \frac{\partial^2 P}{\partial x^2} + K_{zz} \frac{\partial^2 P}{\partial z^2} = 0. \tag{18}$$

And for flow through a deformable medium:

$$\frac{\partial K_{xx}}{\partial x} \frac{\partial P}{\partial x} + K_{xx} \frac{\partial^2 P}{\partial x^2} + \frac{\partial K_{zz}}{\partial z} \frac{\partial P}{\partial z} + K_{zz} \frac{\partial^2 P}{\partial z^2} = 0. \tag{17}$$

Equation (17) is a second-order, partial differential equation with variable coefficients. $\underline{K}_{xx}$ and $\underline{K}_{zz}$ vary throughout the mat. The permeability at any point is dependent on the porosity at that point, which in turn is a function of the compacting pressure on the fibers at that point. The only feasible method of solving such a complicated system is through the use of a numerical method using an automatic digital computer. The same method will be completely satisfactory for solving Equations (18) and (19), with several simplifications being possible.

Many different numerical methods for solving such partial differential equations exist. The method chosen for this study was a simple finite difference approximation of the differential equation. This was chosen mainly because of its ready adaptation

for use with a digital computer and because of the fact that satisfactory results using this method have been obtained for similar flow problems.

The first step in such a solution is to convert the partial differential equation into a set of partial difference equations. The central finite difference approximations for the first and second derivatives of the function $\underline{P}$ are given below:

$$\frac{\partial P}{\partial x} = (P_{i+1,j} - P_{i-1,j})/2h \tag{24}$$

$$\frac{\partial^2 P}{\partial x^2} = (P_{i+1,j} - 2P_{i,j} + P_{i-1,j})/h^2. \tag{25}$$

Here $\underline{h}$ is the finite difference interval or mesh spacing. When these approximations are introduced into Equation (17), the following finite difference equation is obtained:

$$\begin{aligned} 1/4 \Big[& (K^x_{i+1,j} - K^x_{i-1,j})(P_{i+1,j} - P_{i-1,j}) \\ & + (K^z_{i,j+1} - K^z_{i,j-1})(P_{i,j+1} - P_{i,j-1}) \Big] \\ & + K^x_{i,j}(P_{i+1,j} - 2P_{i,j} + P_{i-1,j}) \\ & + K^z_{i,j}(P_{i,j+1} - 2P_{i,j} + P_{i,j-1}) = 0. \end{aligned} \tag{26}$$

The introduction of these approximations into Equation (18) gives the finite difference equation governing flow in anisotropic nondeformable media.

$$\begin{aligned} & K^x (P_{i+1,j} - 2P_{i,j} + P_{i-1,j}) \\ & + K^z (P_{i,j+1} - 2P_{i,j} + P_{i,j-1}) = 0. \end{aligned} \tag{27}$$

Here $\underline{K^x}$ and $\underline{K^z}$ are constant, but not equal. Finally for an isotropic medium, the

partial difference equation approximating Equation (19) is

$$P_{i+1,j} + P_{i-1,j} + P_{i,j+1} + P_{i,j-1} - 4P_{i,j} = 0. \qquad (28)$$

PROGRAMMING THE DIFFERENCE EQUATIONS FOR THE COMPUTER

There are many iterative methods for numerically solving the difference equations. They vary in many respects, including their applicability to use on automatic computers, simplicity of programming, required computing time, and required computer storage space. The successive-overrelaxation method was chosen because of its simplicity, combined with its relatively small requirements on computer time and especially on storage space. In the following section is a brief outline of this iterative procedure. [For the sake of simplicity, Equation (28) will be used to illustrate the application of the iterative procedure. However, its use in the more general case [Equation (26)] is completely analogous.]

First the experimental region is overlayed with a square mesh (mesh spacing = $\underline{h}$) as illustrated in Fig. 20. The pressure at each mesh point is represented by

$$P_{i,j} \qquad i = 1,2,\ldots,n \quad ; \quad j = 1,2,\ldots,m.$$

Equation (28) is then rewritten in the form

$$P_{i,j} = 1/4\ (P_{i+1,j} + P_{i-1,j} + P_{i,j+1} + P_{i,j-1}). \qquad (29)$$

This expresses the pressure at any mesh point as the average of its four nearest neighbors. In solving the system, boundary values are introduced along with an initial estimation of the values of the interior mesh points. Equation (29) is then used to obtain new values of the interior points and this process is repeated for all the interior points of the region until the value of each point differs from the previous estimation of that value by less than some predetermined small number. Thus, an

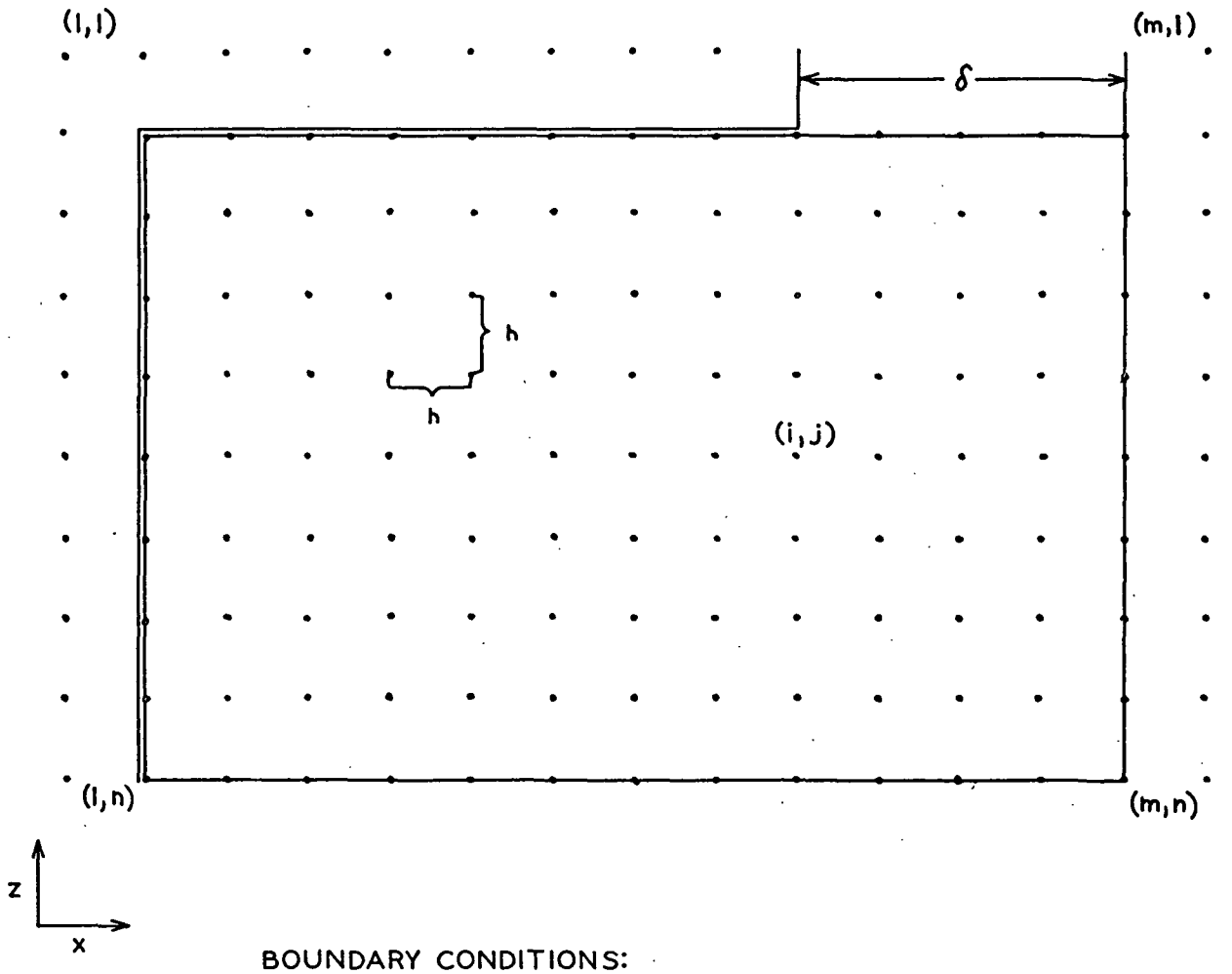

BOUNDARY CONDITIONS:

$$P(i,n) = 0$$

$$P(i,2) = \Delta P \quad \text{FOR} \quad m \geq i \geq m - \left(\frac{\delta}{h} + 1\right)$$

$$P(i,j) = P(3,j)$$

$$P(m,j) = P(m-2,j)$$

$$P(i,1) = P(i,3) \quad \text{FOR} \quad 1 < i < m - \left(\frac{\delta}{h} + 1\right)$$

Figure 20. Experimental System Overlayed with a Square Mesh

estimation of the pressure distribution within the experimental system is obtained. A more accurate estimation can be obtained by reducing the mesh spacing and repeating the iteration cycle. In the absence of truncation error, the solution of the partial difference equation will approach the true solution of the partial differential equation as the mesh spacing approaches zero.

The above iteration technique is generally referred to as the Gauss-Seidel method. It is extremely well adapted for use on a digital computer. However, this method has the disadvantage of being rather slow to converge, thus requiring excessive machine time. The successive-overrelaxation method is a simple modification of the above technique which greatly increases the rate of convergence. Using this method, Equation (28) is written in the form

$$P_{i,j}\ (\text{new}) = (1-\omega)\ P_{i,j}\ (\text{old}) + 1/4\omega\ (P_{i+1,j} + P_{i-1,j} + P_{i,j+1} + P_{i,j-1}) \tag{30}$$

where

ω = relaxation parameter $\qquad (1 \leq \omega < 2)$.

If $\omega = 1$, there is no overrelaxation and Equation (30) reduces to the Gauss-Seidel method. However, for $1 < \omega < 2$, there is some optimum value of ω for which the most rapid rate of convergence is obtained. Lapidus (45) gives the following method of Frankel and Young for finding this optimum value of ω. According to these authors, the value of ω calculated from solving Equation (31) for the smallest root is an optimum value.

$$\omega^2 t^2 - 16\omega + 16 = 0 \tag{31}$$

where

$\underline{t} = 2 \cos [\pi/(\underline{N} + 1)]$

$\underline{N}$ = the number of elements in one column or one row of a square matrix.

This relation was derived for the Laplace equation and a square array. It should also be applicable to a rectangular array of n rows and m columns where $N = \sqrt{mn}$. Although not strictly applicable to an equation other than Laplace's, the method is still very useful because any ω near ω_{opt} will yield greatly improved convergence.

To check the validity of the above relation for this experimental system, Equation (30) was solved using different values of ω and the number of iterations necessary for convergence were noted. These results are shown in Fig. 21. The value of ω_{opt} as calculated from the Frankel and Young relation lies on the minimum of the curve. About a threefold decrease in convergence time is attained by using the successive-overrelaxation method rather than the Gauss-Seidel method ($\omega = 1.0$). Figure 22 is a block diagram outlining the basic iteration cycle of the computer program.

BOUNDARY AND INITIAL CONDITIONS

BOUNDARY CONDITIONS

A set of boundary values and initial conditions must be known in order to solve the finite difference equations for the pressure distribution. The boundary conditions are chosen to describe the experimental system which is to be simulated. As stated earlier, this system consists of a fibrous mat with one face fully open to flow while only a slot in the middle of the opposite face is open to flow. This was illustrated in Fig. 6. The boundary conditions consist of a constant pressure of zero at the open face and a constant pressure of ΔP (the total pressure drop) at the slot. At the walls of the filtration tube there is no normal velocity component so that the normal derivative of the pressure at the walls is zero. Since the system is symmetrical, only one-half of the mat need be considered, along with the added boundary condition that the normal derivative of the pressure along the center line is zero.

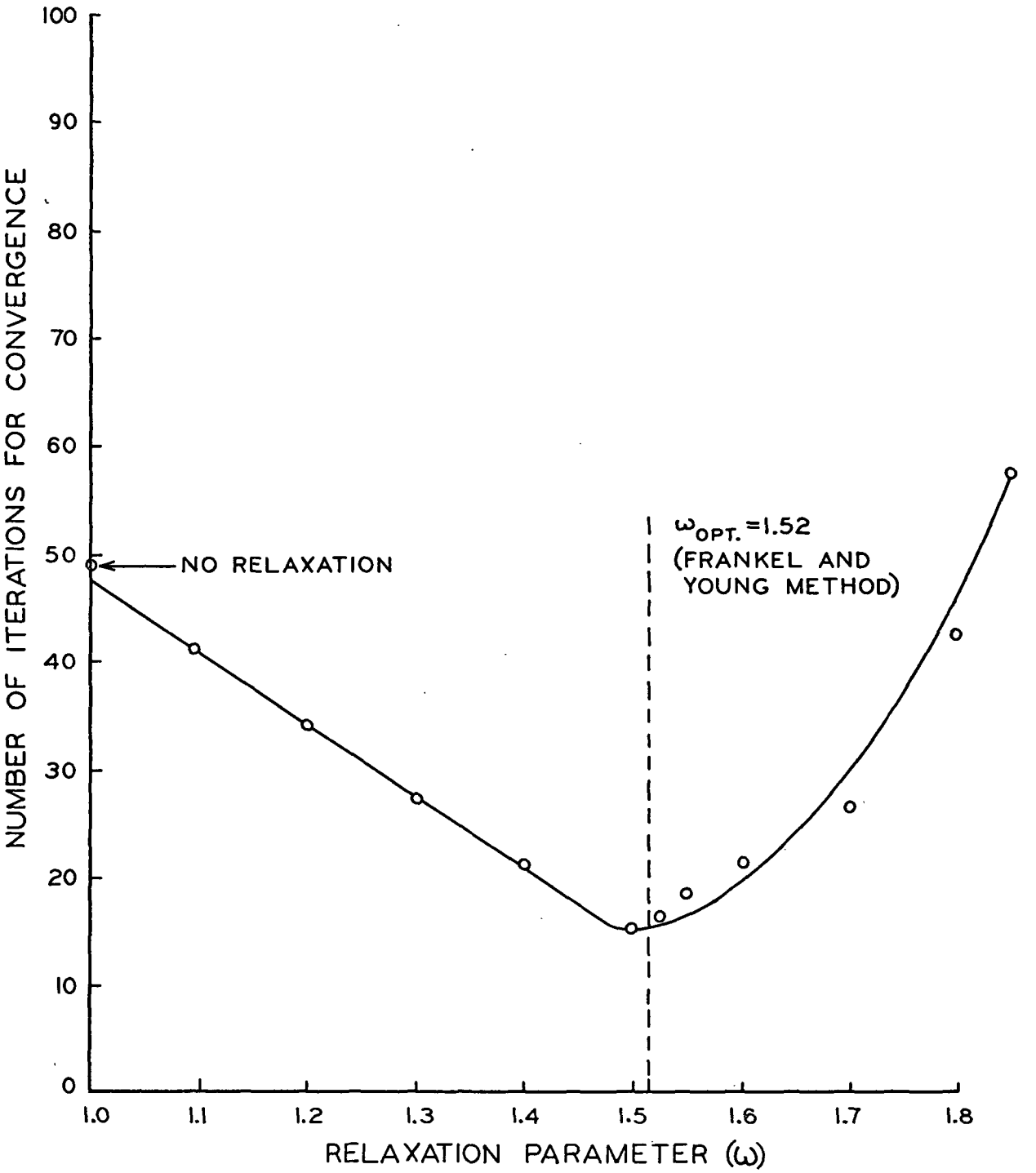

Figure 21. Optimum Relaxation Parameter (Successive-Overrelaxation Iteration Procedure)

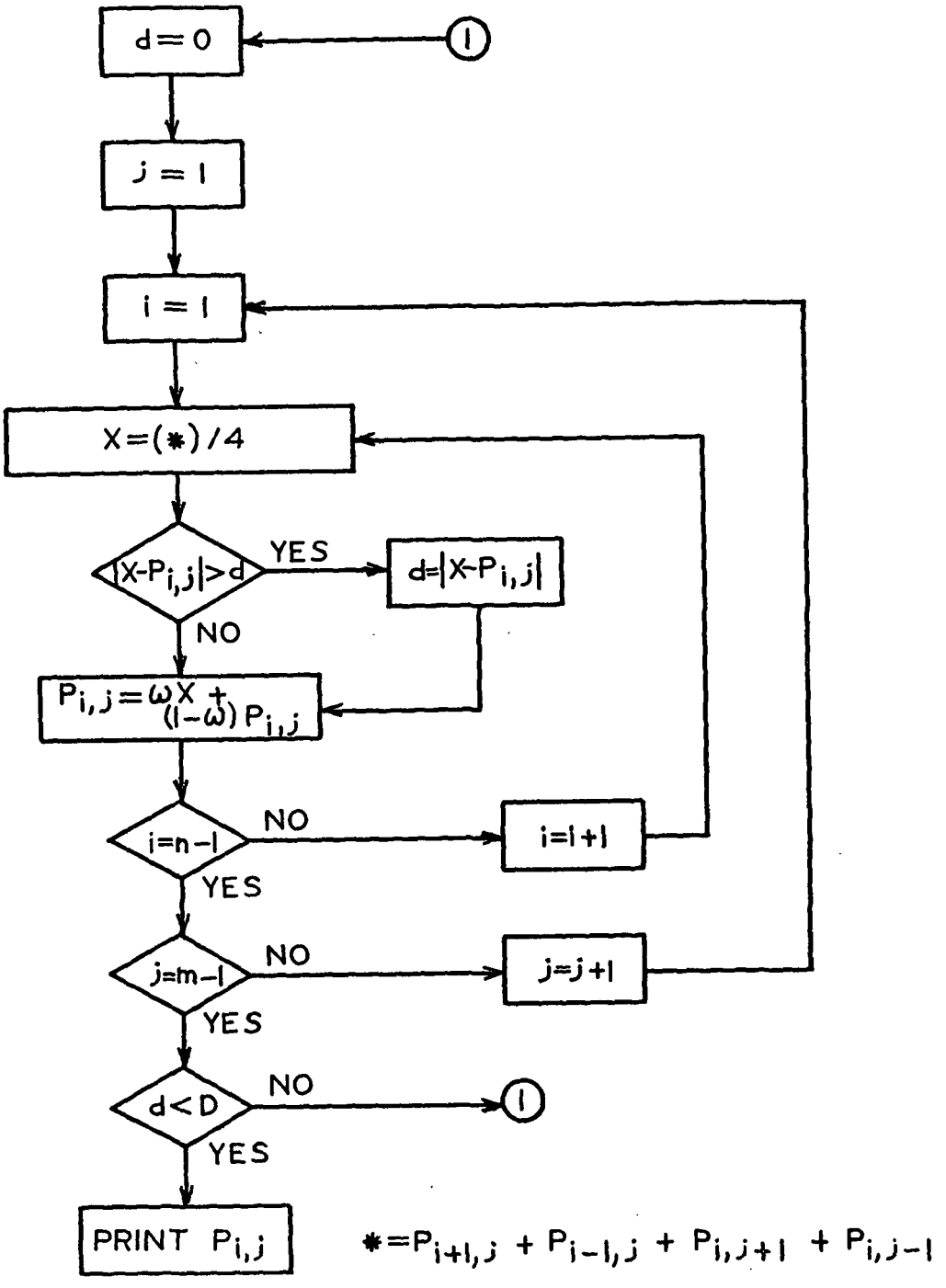

Figure 22. Block Diagram of Basic Iteration Cycle (Successive-Overrelaxation Method)

In applying these boundary conditions to the finite difference equations, points on the mat face and at the slot are assumed to have pressures of zero and ΔP, respectively. At the boundaries where the normal pressure gradient is zero, the so-called "reflection" boundary conditions described by Douglas and Peaceman (46) are applicable. In using the "reflection" boundary conditions, a set of fictitious points are imagined to exist at a distance h outside the boundary. These points are assumed to have the same values as the points located a distance h inside of the boundary.

Figure 20 shows the experimental system with the assigned set of boundary conditions. These conditions are summarized at the bottom of the figure.

INITIAL CONDITIONS

The choice of initial conditions is not critical. The numerical solution should be the same, no matter what initial conditions are used. Often in iterative solutions of this type, all the interior points are assigned a value of zero. However, faster convergence is obtained if interior points with values close to the final values are chosen. Thus, as a first approximation, a linear pressure drop in the transverse direction through the mat was usually assumed. If a better approximation was known, such as a preliminary pressure distribution, then this was used.

PERMEABILITY AND COMPRESSIBILITY RELATIONSHIPS

In the preceding sections of the Appendix, the use of the iteration procedure for the solution of the finite difference equations was illustrated using Laplace's equation. Thus, permeability and compressibility relations were not involved, for Laplace's equation is valid only for flow through isotropic, nondeformable media. However, for the more general case of two-dimensional flow through deformable media, as represented by Equation (17) or Equation (26), both the permeability and compressibility relationships are most important.

As shown in the introduction, there are many theoretical and empirical permeability functions. It was found experimentally that the permeability data of this study best fit an empirical correlation of the Davies-Ingmanson type. In this correlation, the permeability may be represented by

$$K = \frac{1}{\mu S_v^2 k_1 (1-\varepsilon)^{3/2}[1 + k_2(1-\varepsilon)^3]} . \qquad (32)$$

For transverse flow (K^z): $k_1=3.5$; $k_2=57.0$.
For lateral flow (K^x): $k_1=2.8$; $k_2=50.0$.

Thus, the permeability is a rather complex function of the porosity. The porosity, however, is not constant, but rather is dependent on the compressibility of the fibrous system and the compacting pressure on the fibers. Therefore, a compressibility function must be included in the differential equations describing flow.

For two-dimensional flow, to be complete, the compressibility in both directions of flow, along with the interactions of these compressibility functions would have to be taken into account. This is an exceedingly complex problem. The transverse compressibility can be measured fairly easily, but the measurement of the lateral compressibility would be very difficult. Measurement of the interaction of these two compressibilities, that is the effect that lateral compression would have on the transverse compressibility and vice versa, would involve an even higher degree of complexity. Even if these quantities could be determined experimentally, their introduction into the already complicated difference equations describing two-dimensional flow would almost surely produce a problem too complex to be solved on the computer available for this study.

The only practical course at this time appeared to be to develop an expression for the compressibility in the major direction of flow (transverse) and to neglect for the present the lateral compressibility and any interactions. This approach

is not totally without merit because the lateral compressibility is probably quite a bit smaller than the transverse compressibility in the present system. In addition, the forces causing compression are generally smaller in the lateral direction. Thus, although it is recognized that to be rigorous stress must be considered a tensor, this study considers it in only one direction in order to obtain an approximate analytical solution.

The simplest compressibility function has the form

$$c = M P_f^N = (1-\varepsilon)\rho_f \qquad (6)$$

where

$\underline{c}$ = mat density

$\underline{P_f}$ = compacting pressure on the fibers

$\underline{M},\underline{N}$ = compressibility constants

$\rho_{\underline{f}}$ = fiber density

ε = porosity

The compressibility constants are determined from a static compressibility test in which a homogeneous fiber mat is subjected to a uniform compacting load. It is then assumed that these constants apply to the dynamic case where the compacting pressure on the fibers is due to fluid flow rather than mechanical loading. However, when the compacting pressure is due to fluid flow, there is no longer a uniform concentration in the fiber mat, but rather there is a distribution of concentration ranging from a minimum at the open face of the mat to a maximum at the septum.

This compressibility function can thus be used to find the porosity at any point within the mat if the compacting pressure on the fibers at that point is known. Considering only forces in the $\underline{z}$-direction, the compacting pressure $\underline{P_f}$ is related to the hydrostatic pressure $\underline{P}$ by the equation

$$\frac{\partial P_f}{\partial z} = -\frac{\partial P}{\partial z} . \tag{33}$$

Integration of this equation yields

$$P - P_0 = P_{f,0} - P_f \tag{34}$$

and

$$P - P_L = P_{f,L} - P_f = -P_{i,j} \tag{35}$$

where $\underline{L}$ refers to the open face and 0 refers to the septum. In the unconfined mat subject to fluid flow, $P_{\underline{f},\underline{L}} = 0$. Therefore $P_{\underline{f}} = P_{\underline{i},\underline{j}}$. Thus, the compacting pressure on the fibers at any point is just equal to the pressure due to flow at that point.

In the present experimental system, however, the mat is compressed to some initial porosity $\varepsilon_{\underline{I}}$ with a piston and then the pressure drop due to fluid flow is measured. This flow causes a change in the porosity distribution, resulting in porosities higher than $\varepsilon_{\underline{I}}$ where the fluid enters the mat and porosities lower than $\varepsilon_{\underline{I}}$ where it leaves. Thus, if $P_{\underline{I}}$ is the initial pressure, then during flow

$$P_{f,L} < P_I \qquad \text{(septum)} \tag{36}$$

$$P_{f,0} > P_I \qquad \text{(slot)} \tag{37}$$

Rearranging Equation (35), the compacting pressure on the fibers at any point within the mat is given by

$$P_f = P_{f,L} + P_{i,j} \tag{38}$$

$P_{\underline{i},\underline{j}}$ is the pressure at any point within the mat due to fluid flow and is obtained from the numerical solution of the flow equation. Thus, if a relationship to describe $P_{\underline{f},\underline{L}}$ can be found, this equation will provide a means of determining the compacting pressure on the fibers at any point within the mat.

In deriving this relationship for $P_{f,L}$, it is first useful to investigate the limits on $P_{f,L}$ and determine what values of the total overall pressure drop will produce these limits. First, when there is no flow (total pressure drop $\Delta P_t = 0$)

$$P_{f,L} = P_f = P_I. \tag{39}$$

This states that when no flow is occurring, the compressive pressure on the fibers is uniform throughout the mat and is equal to the initial pressure applied by the piston. Also, at some maximum total pressure drop ΔP_{Max}, the fibers will lift away from the lower boundary so that

$$P_{f,L} = 0. \tag{40}$$

It is thus necessary to estimate the maximum total pressure drop. It can be obtained by finding the total pressure drop across an unconfined mat of the same thickness and with the same total mass as the confined mat. For mats of similar total mass and thickness, the average concentration $\bar{c}$ within the mat subject to fluid forces is equal to the initial concentration c_I of the mechanically loaded mat.

It has been reported (47) that for an unconfined mat under fluid stress, for the relatively high porosities encountered in this study, the average concentration $\bar{c}$ can be approximated by

$$\bar{c} = (1 - N/2)^2 M \mid \Delta P_{Max} \mid^N. \tag{41}$$

Also, from the static compressibility equation

$$c_I = M \mid P_I \mid^N. \tag{42}$$

Equating these two relationships, the following is obtained:

$$(1 - N/2)^2 M \mid \Delta P_{Max} \mid^N = M \mid P_I \mid^N \tag{43}$$

or

$$\Delta P_{Max} = \left[\frac{1}{(1 - N/2)^2}\right]^{1/N} \cdot P_I. \qquad (44)$$

This indicates that the maximum fluid pressure drop needed to cause the confined mat to lift away from the lower surface is a function of the initial compression ($\underline{P_I}$) and of the compressible nature of the fiber mat ($\underline{N}$). Introducing the value of the compressibility constant ($\underline{N}$ = 0.267) applicable for the experimental system this equation becomes

$$\Delta P_{Max} = 2.90 \cdot P_I. \qquad (45)$$

Thus, at a total pressure drop of approximately 2.9 times the initial compacting pressure, the fiber mat will lift away from the lower surface and $\underline{P_{f,L}}$ will be zero. These limiting boundary conditions are summarized below:

when $\Delta P_t = 0$; $P_{f,L} = P_{f,0} = P_f = P_I$

when $\Delta P_t = \Delta P_{Max}$; $P_{f,L} = 0$, $P_{f,0} = \Delta P_{Max}$.

It will be recalled that an equation has already been derived for the compressive pressure on the fibers at any point $\underline{P_f}$ in terms of the pressure at the lower surface $\underline{P_{f,L}}$ and the pressure at that point due to fluid flow $\underline{P_{i,j}}$. That equation is

$$P_f = P_{f,L} + P_{i,j}. \qquad (38)$$

It is now also known that the limiting boundary conditions restrict $\underline{P_{f,L}}$ to values between zero and $\underline{P_I}$. Physically, the pressure on the fibers at the lower surface $\underline{P_{f,L}}$ is due to the initial compacting pressure minus a quantity which represents the relief of some of this initial compacting pressure by the fluid stresses. The amount of this relief is dependent on the total pressure drop due to fluid flow across the mat at that position. Thus

$$P_{f,L} = P_I - C\,\Delta P_t. \tag{46}$$

Applying the two limiting boundary conditions, this becomes

$$P_{f,L} = P_I - \Delta P_t/2.9. \tag{47}$$

Introducing this into Equation (38), the expression for the compressive pressure on the fibers at any point within the mat is obtained.

$$P_f = P_I - \Delta P_t/2.9 + P_{i,j} \tag{48}$$

where

$\underline{P_f}$ = compacting pressure on the fibers at any point $\underline{i,j}$ within the mat

$\underline{P_I}$ = initial pressure applied by the piston

$\underline{\Delta P_t}$ = total pressure drop across the mat due to fluid flow (at fixed values of $\underline{x}$)

$\underline{P_{i,j}}$ = pressure at any point $\underline{i,j}$ due to fluid flow

Substituting this equation into Campbell's compressibility function yields

$$c = (1-\varepsilon)\rho_f = M\,(P_I - \Delta P_t/2.9 + P_{i,j})^N. \tag{49}$$

This is the final form of the equation used to relate pressure to porosity and thus ultimately to permeability. It must be remembered that this equation was obtained from a one-dimensional treatment of the fluid stresses within the fiber mat. It does seem to describe the experimental system where lateral compression is small. However, for systems with significant lateral compression, it is probably not applicable. For such a system, the tensorial nature of the stresses within the system would have to be taken into account.

ANALYSIS OF COMPUTATION ERRORS

There are two types of errors involved in solving elliptic partial differential equations such as Equations (17), (18), and (19) by the iterative method outlined above.

The first type of error arises in the solution of the finite difference equations themselves. For rectangular boundaries this error is largely round-off error. Since the iteration can be carried to as many significant figures as desired, this type of error is usually insignificant. For the system in this study, the round-off error in the flow rate or apparent permeability values was found to be less than 0.01%.

The second type of error is the truncation error resulting from replacing the partial differential equation with the difference approximation. With the central differences used in the difference equations, this truncation error was reported to be proportional to h^2 where h is the grid spacing (48). Figure 23 shows values of the flow rate computed at several different grid spacings and indicates that the assumption of the error being proportional to the square of the grid spacing is valid.

An estimate of the magnitude of this error can be obtained by comparing calculated values obtained with two different grid spacings. This procedure is illustrated below:

$$Q_1 = Q_{true} + c\, h_1^2 \qquad (50)$$

$$Q_2 = Q_{true} + c\, h_2^2 \qquad (51)$$

here

Q_1, Q_2 = calculated values of the flow rate

Q_{true} = true value of the flow rate (unknown)

h_1, h_2 = grid spacings

c = constant (unknown)

These two equations are solved simultaneously for Q_{true}. Then the truncation error is determined by the equation

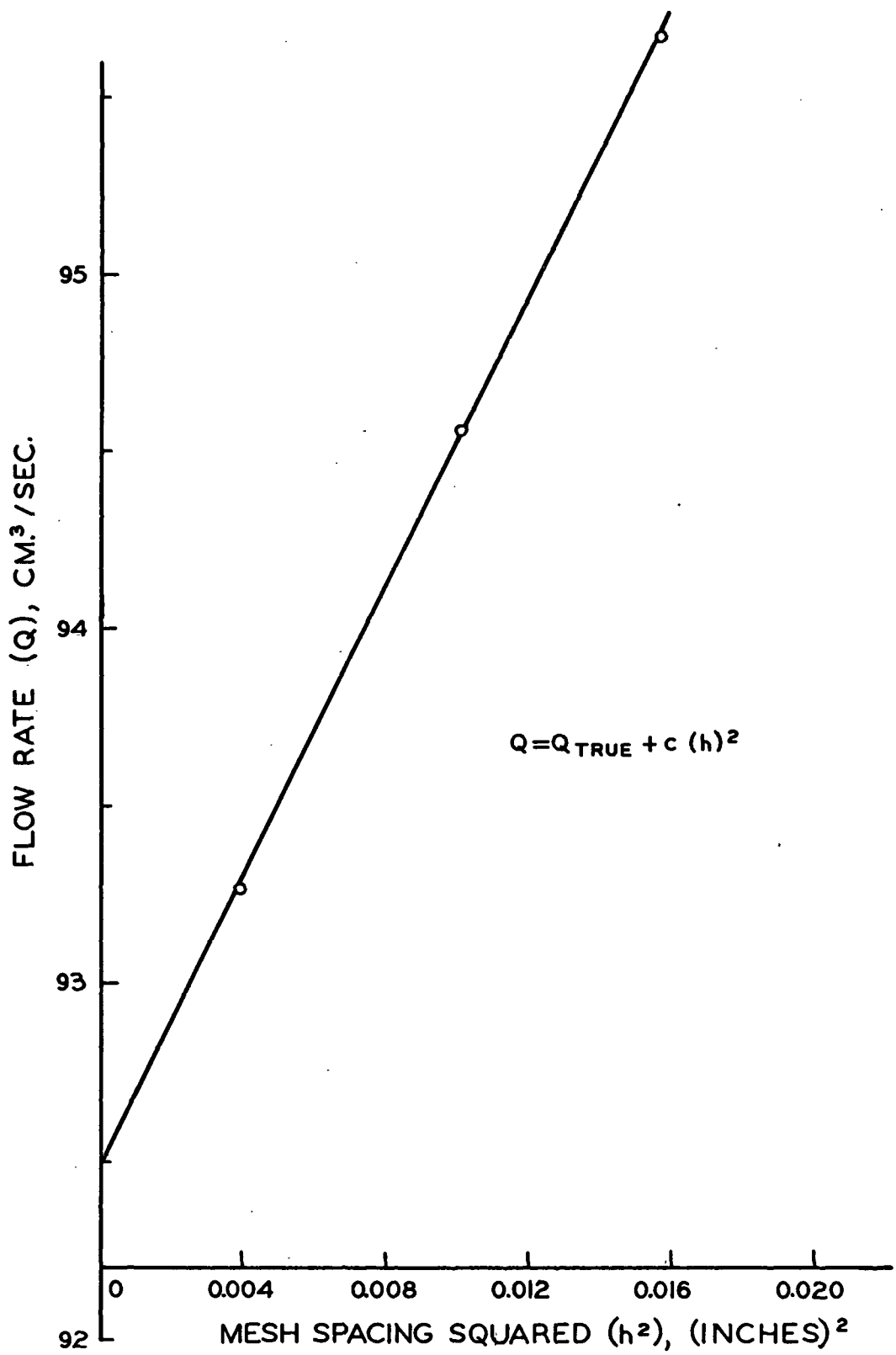

Figure 23. Truncation Error

$$\% \text{ error} = \frac{Q_1 - Q_{true}}{Q_{true}} \times 100\%. \qquad (52)$$

The magnitude of the truncation error found in this study is shown in Table III for two grid spacings and three slot widths.

TABLE III

TRUNCATION ERRORS

Grid Spacing	Slot Width, %		
	1 inch	1/2 inch	1/4 inch
1/8 inch	3.5	5.2	7.5
1/16 inch	0.9	1.3	2.0

It is evident from Table III that there is less truncation error when a smaller grid spacing is used. However, a smaller grid spacing produces a larger number of grid points and results in a correspondingly longer computing time. For flow through deformable media, the computer time necessary to obtain one pressure distribution at a mesh spacing of 1/8 inch was 1-2 hours. If this grid spacing was decreased by one-half, to 1/16 inch, more than ten hours was needed to obtain the pressure distribution. Thus, to cut down on the necessary computer time, the bulk of the computations was carried out using the coarse grid spacing. Then these results were corrected using the error estimates found in Table III.

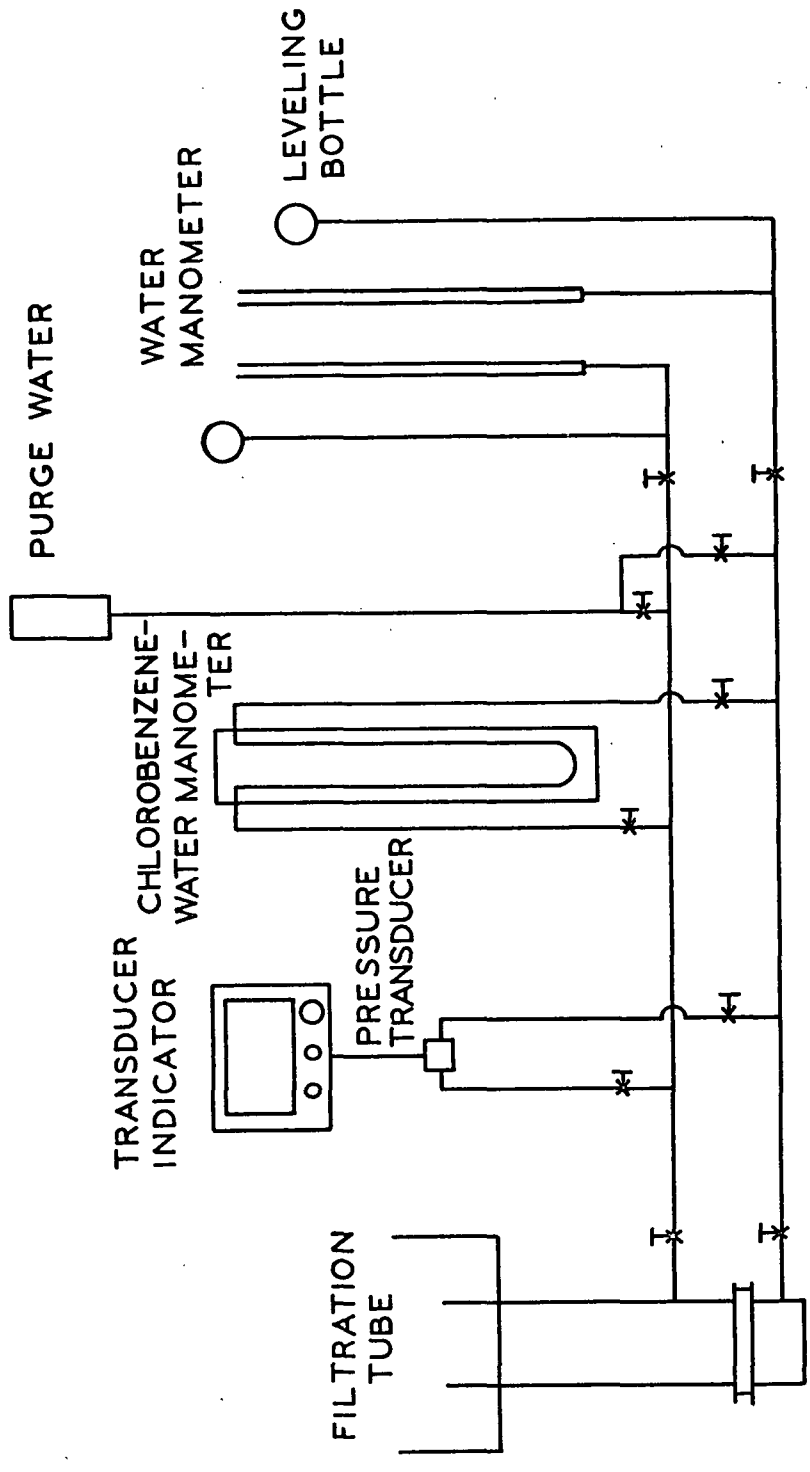

Figure 24. Pressure Measuring System

APPENDIX III

CORRELATION OF PRESSURE DROP-FLOW RATE DATA AT VARYING POROSITIES

Experimental data on two-dimensional flow through deformable porous media were obtained at several different porosities for each of the three slot widths. A method was then sought to correlate all of the pressure drop-flow rate data for a particular system. In examining some of the numerical data from the computer solutions, it appeared that comparing the flow rates at the same values of the relative pressure drop ($\Delta P_t / \Delta P_{Max}$) would be helpful. ($\Delta P_t$ = total pressure drop across the mat and ΔP_{Max} = total pressure drop at which the fiber mat lifts away from its confinements.) This comparison seemed logical because the same percentage of the maximum pressure drop should produce the same percentage change in the porosity distribution, resulting in a similar percentage change in the overall flow rate Q. This suggests that, for similar systems, at the same relative pressure drops, the relative pressure distributions within the systems should be identical no matter what the average porosities of the systems. This is evident in Fig. 25. The three systems in this figure have the same geometry but different average porosities. The lower two systems, compared at the same relative pressure drops, have identical relative pressure distributions. The upper system, compared at a different relative pressure drop, shows a very different pressure distribution. Thus, this appears to justify comparing the systems at the same relative pressure drops.

Flow rate values compared at similar relative pressure drops will still not be the same because there are differences in the average porosities of the systems. Thus, a factor must be included to correct for these differences in average porosity. The proper factor may be found by investigating Darcy's law written for the overall system. This equation, written for average porosities of ε_1 and ε_2, is shown as follows:

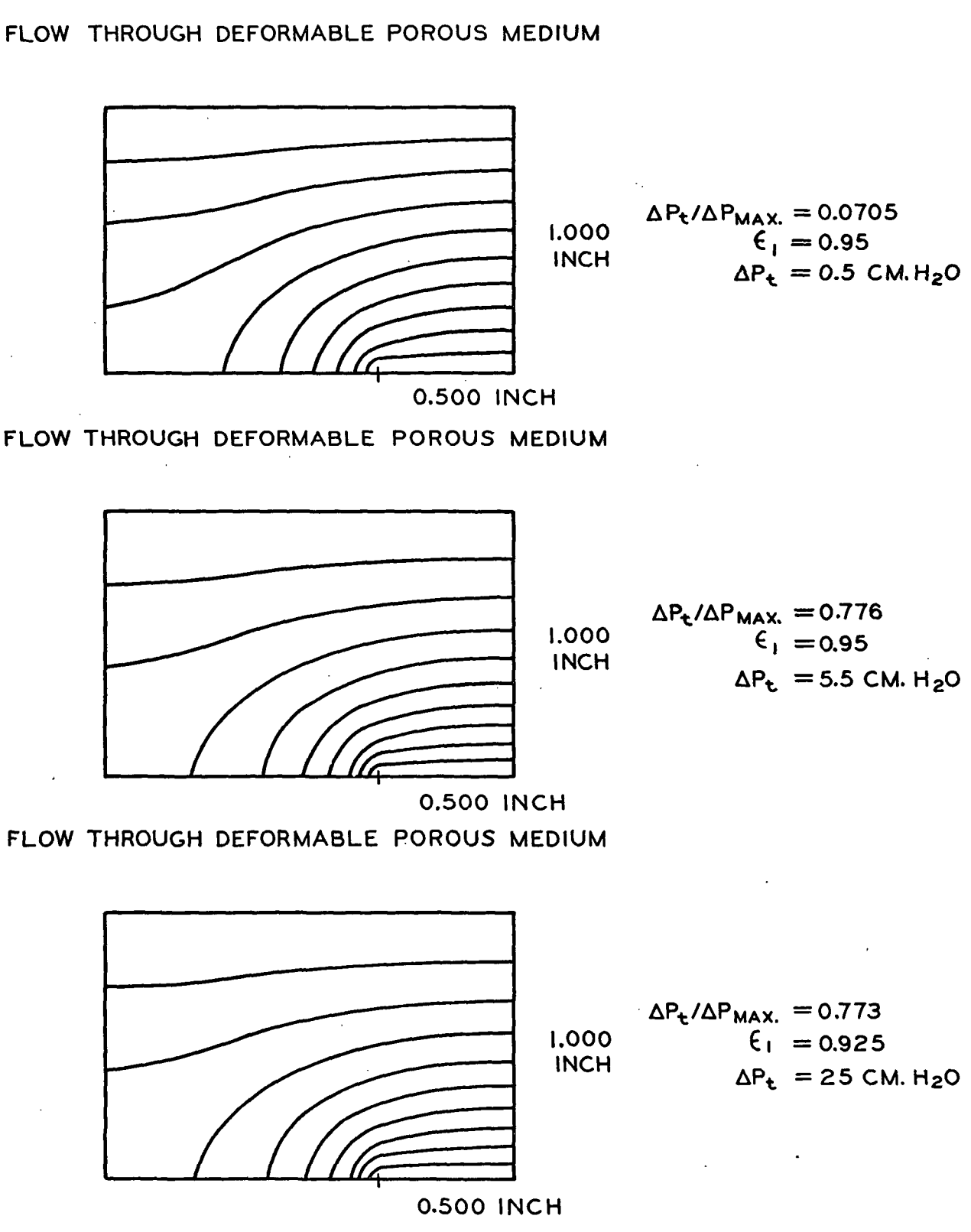

Figure 25. Comparison of Pressure Distributions at Similar Relative Pressure Drops

$$Q_{\varepsilon_1} = K_{App\varepsilon_1} \frac{A\Delta P_{t\varepsilon_1}}{L} \tag{53}$$

$$Q_{\varepsilon_2} = K_{App\varepsilon_2} \frac{A\Delta P_{t\varepsilon_2}}{L} \tag{54}$$

Introducing the relative pressure drops into these expressions, they become

$$Q_{\varepsilon_1} = K_{App\varepsilon_1} \frac{A}{L} \frac{\Delta P_{t\varepsilon_1}}{\Delta P_{Max\varepsilon_1}} \Delta P_{Max\varepsilon_1} \tag{55}$$

$$Q_{\varepsilon_2} = K_{App\varepsilon_2} \frac{A}{L} \frac{\Delta P_{t\varepsilon_2}}{P_{Max\varepsilon_2}} \Delta P_{Max\varepsilon_2} \tag{56}$$

Then dividing Equation (61) by Equation (62), the following equation is obtained:

$$\frac{Q_{\varepsilon_1}}{Q_{\varepsilon_2}} = \frac{(\Delta P_{t\varepsilon_1}/\Delta P_{Max\varepsilon_1})}{(\Delta P_{t\varepsilon_2}/\Delta P_{Max\varepsilon_2})} \cdot \frac{K_{App\varepsilon_1}}{K_{App\varepsilon_2}} \cdot \frac{\Delta P_{Max\varepsilon_1}}{\Delta P_{Max\varepsilon_2}} . \tag{57}$$

At the same relative pressure drop, this equation becomes

$$\frac{Q_{\varepsilon_1}}{Q\varepsilon_2} = \frac{K_{App\varepsilon_1}}{K_{App\varepsilon_2}} \frac{\Delta P_{Max\varepsilon_1}}{\Delta P_{Max\varepsilon_2}} \tag{58}$$

Or rearranging this expression

$$\frac{Q_{\varepsilon_1}}{K_{App\varepsilon_1} \cdot \Delta P_{Max\varepsilon_1}} = \frac{Q_{\varepsilon_2}}{K_{App\varepsilon_2} \cdot \Delta P_{Max\varepsilon_2}} = \text{constant.} \tag{59}$$

Thus, if $\underline{Q}/(\underline{K}_{App} \cdot \Delta \underline{P}_{Max})$ is plotted versus $(\Delta \underline{P}_{\underline{t}}/\Delta \underline{P}_{Max})$, the data for all values of ε should fall on the same line. This was found true for both the experimental and computed pressure drop-flow rate data.

APPENDIX IV

OVERALL OR APPARENT PERMEABILITY IN THE TWO-DIMENSIONAL SYSTEM

The overall or apparent permeability in the two-dimensional system is not a true permeability. It is an average measure of the overall properties of the system, taking into account both the permeability properties of the porous medium and the geometry of the system. Perhaps the following development will reveal a little more clearly how the apparent permeability depends on these properties.

First consider a differential slice of the porous medium as shown in Fig. 26. Darcy's law can be written

$$u = -K \frac{dP}{dz}. \tag{60}$$

Integrating both sides of this equation over a differential element of area $\underline{dz} \cdot \underline{dx}$ yields

$$\int_0^L \int_0^{b_o} u \, dz \, dx = - \iint K \frac{dP}{dz} \, dz \, dx \tag{61}$$

$$L \, b_o U_o = - \int_0^{b_o} \int_{P_o(x)}^{P_1(x)} K(P) \, dP \, dx \tag{62}$$

$$L \, b_o U_o = - \int_0^{b_o} \overline{K} \, (P_1(x) - P_o(x)) \, dx \tag{63}$$

$$L \, b_o U_o = - \bar{\bar{K}} \, b_o (\overline{P}_1 - \overline{P}_o). \tag{64}$$

But $\underline{(\overline{P}_1 - \overline{P}_o)} = -\underline{\Delta P}$ and $\underline{U_o} = \underline{Q}/\underline{A}$. Therefore

$$Q = \bar{\bar{K}} \frac{A \Delta P}{L} = K_{App} \frac{A \Delta P}{L}. \tag{65}$$

This development indicates that the apparent permeability is an average function, dependent on the pressure distribution within the medium. This in turn is dependent on system geometry and porosity distribution.

A transformation based on conformal mapping of the experimental region would allow the integrations to show the effect of slot width. However, this would only be possible for a nondeformable medium where $\underline{K}$ was independent of pressure. Also, complications would occur at the corners of the slot where there would be a tendency for a jet to form.

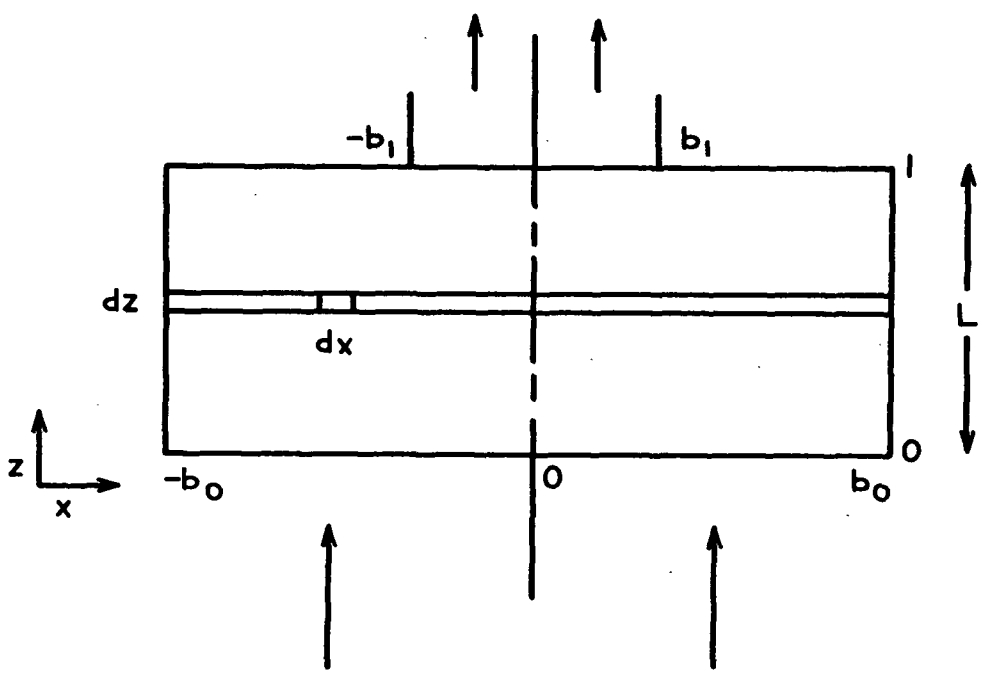

Figure 26. Experimental System Showing a Differential Element of Area $\underline{dz} \cdot \underline{dx}$

APPENDIX V

EXPERIMENTAL AND COMPUTER DATA

DETERMINATION OF FIBER SPECIFIC SURFACE AREA (S_v)

Fiber specific surface area was determined from microscopic fiber diameter measurements. These measurements were made on fibers suspended in water to account for any swelling. For cylindrical fibers, the specific surface is equal to four times the inverse of the fiber diameter.

Fiber diameter determinations were made on 100 fibers at a magnification of 400X. The fibers were mounted in water to account for the slight swelling of nylon in water. Table IV gives this fiber diameter information.

TABLE IV

FIBER DIAMETER DETERMINATION

Fiber Diameter x 10^4, cm. (a)	Frequency, % (b)	($a \cdot b$)
15.08	1	15.08
16.24	6	97.44
17.40	13	226.20
18.56	26	482.56
19.72	16	315.52
20.88	10	208.80
22.04	5	110.20
23.20	7	162.40
24.36	4	97.44
25.52	4	102.08
26.68	3	80.04
27.84	2	55.68
29.00	2	58.00
30.16	1	30.16
	100	2041.60

Arithmetic average fiber diameter $= \dfrac{(a \cdot b)}{b} = 20.4 \times 10^{-4}$ cm.

Specific surface area (S_v) $= 4/d = 1960$ cm^{-1}.

TABLE V

PHYSICAL PROPERTIES OF THE NYLON FIBERS
(DU PONT NYLON TYPE 227)

Average Fiber Diameter = 20.4×10^{-4} cm.

Specific Surface Area = 1960 $cm.^{-1}$

Approximate Fiber Length = 3 mm.

Fiber Density = 1.14 $g./cm.^3$

Moisture Regain (75°F. and 65% R.H.) = 4%

TABLE VI

FIBER MAT COMPRESSIBILITY

$(\underline{c} = \underline{M}P_f^{\underline{N}})$

Pressure ($\underline{P}_f$) x 10^{-3}, dynes/$cm.^2$	Mat Density ($\underline{c}$), $g./cm.^3$	
	Run No. 6	Run No. 7
8.15	0.0694	0.0713
13.1	0.0824	0.0856
22.9	0.0990	0.0997
37.7	0.1145	0.1156
62.3	0.1308	0.1319
96.4	0.1468	0.1483
145.8	0.1628	0.1636

$\underline{N} = 0.267$; $\underline{M} = 0.00712 \dfrac{(g./cm.^3)}{(dynes/cm.^2)^{\underline{N}}}$

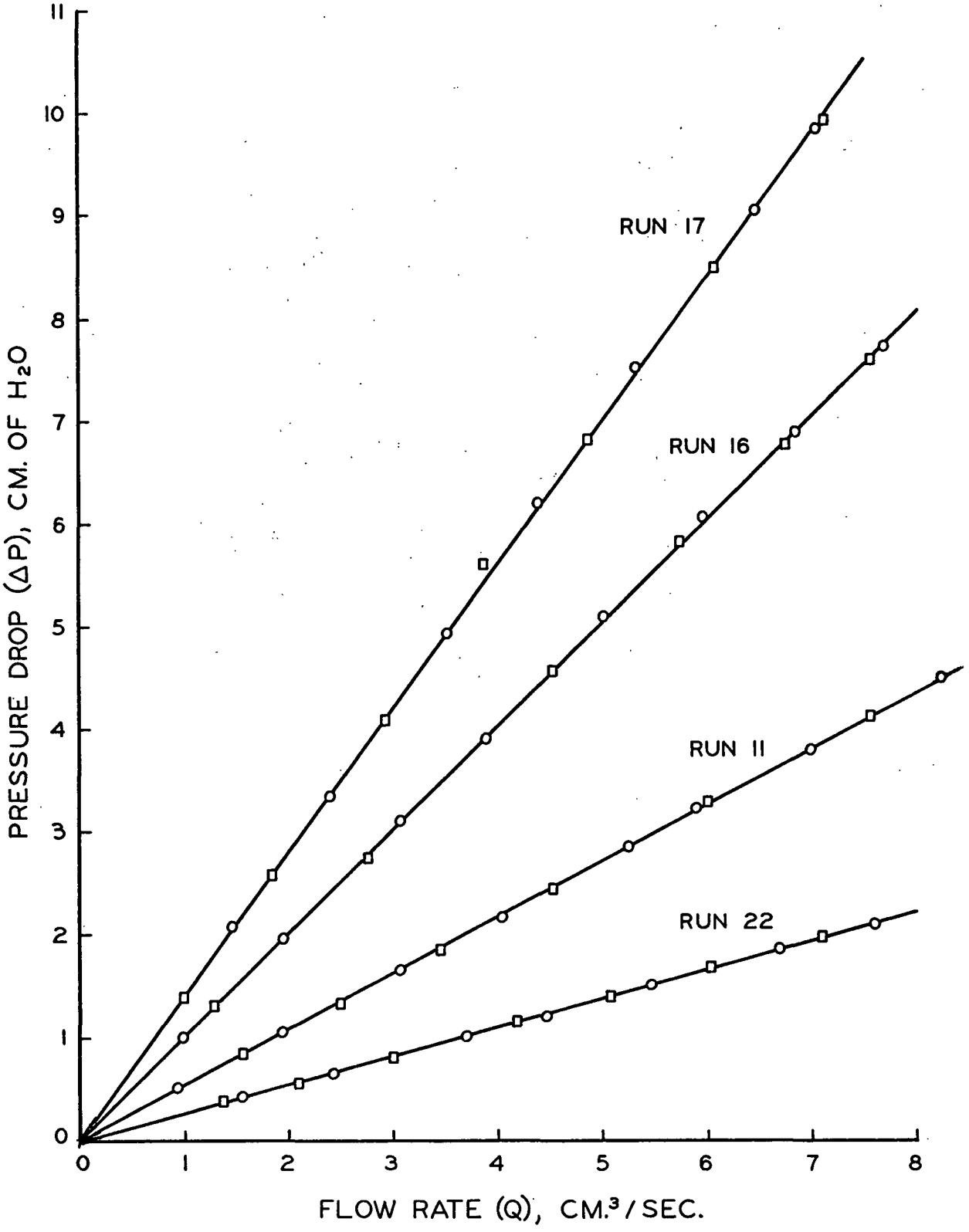

Figure 27. Basic Lateral Permeability Data

TABLE VII

PERMEABILITY AND KOZENY FACTORS FOR TRANSVERSE FLOW THROUGH NYLON FIBER MATS

Run Number	ε	μ, cp.	$\underline{K} \times 10^3$, $\left(\frac{\text{cm.}\cdot\text{sec.}}{\text{g./cm.}^2}\right)$	$\underline{k}$[a]
	0.9527	0.9402	0.8026	13.338
	0.9405	0.9446	0.5423	11.946
	0.9203	0.9446	0.3464	9.766
10	0.9066	0.9446	0.2668	8.826
	0.8843	0.9446	0.1848	7.706
	0.8588	0.9446	0.1272	6.886
	0.8305	0.9446	0.0894	6.152
	0.7478	0.9446	0.0393	4.609
	0.9604	0.9810	0.9449	15.870
	0.9532	0.9764	0.7624	13.833
	0.9388	0.9764	0.5095	11.564
11	0.9235	0.9764	0.3596	9.982
	0.9000	0.9764	0.2328	8.352
	0.8693	0.9764	0.1462	7.015
	0.8388	0.9764	0.0980	6.179
	0.7790	0.9764	0.0501	5.155

[a]The data for $\underline{k}$ can be correlated with the equation

$$\underline{k} = \frac{3.5\ \varepsilon^3}{(1-\varepsilon)^{1/2}}[1 + 57(1-\varepsilon)^3].$$

TABLE VIII

PERMEABILITY AND KOZENY FACTORS FOR LATERAL FLOW THROUGH NYLON FIBER MATS

Run Number	ε	μ, cp.	$\underline{K} \times 10^3$ $\left(\frac{\text{cm.}\cdot\text{sec.}}{\text{g./cm.}^2}\right)$	$\underline{k}$[a]
8	0.9434	1.0199	0.6854	9.764
9	0.9548	0.9380	1.0267	11.521
10	0.9516	0.9741	0.9141	10.758
11	0.9418	0.9315	0.7070	9.752
12	0.9254	0.8777	0.5105	8.276
13	0.9195	0.9101	0.4421	7.765
15	0.9143	0.8978	0.3883	7.774
16	0.9135	0.8897	0.3807	7.833
18	0.9042	0.9491	0.3124	7.075
20	0.8922	0.9185	0.2721	6.368
21	0.8939	0.9315	0.2759	6.429
22	0.9608	0.9122	1.3528	12.181
23	0.9389	0.9446	0.6662	9.175
24	0.9640	0.9858	1.3590	13.437
25	0.8735	0.9579	0.2002	5.656
26	0.9381	0.9358	0.6405	9.361
27	0.9685	0.9468	1.720	14.641
28	0.8746	0.9579	0.1926	6.005
29	0.8569	0.9315	0.1630	5.270
30	0.8586	0.9358	0.1640	5.370

[a] The data for $\underline{k}$ can be correlated with the equation

$$\underline{k} = \frac{2.8\ \varepsilon^3}{(1-\varepsilon)^{1/2}} [1 + 50(1-\varepsilon)^3].$$

TABLE IX

COMPUTER DATA ON TWO-DIMENSIONAL FLOW
THROUGH DEFORMABLE POROUS MEDIA

Mat Thickness = 1 inch Slot Width = 1 inch

Porosity (ε)	Relative Pressure Drop ($\Delta P_t / \Delta P_{Max}$)	Adjusted Flow Rate,[a] $Q/(K_{App} \cdot \Delta P_{Max}) \times 10^{-2}$, cm.
	0.016	3.40
	0.053	11.21
	0.105	22.17
0.900	0.158	32.90
	0.210	43.42
	0.316	64.00
	0.473	94.11
	0.631	123.84
	0.016	3.34
	0.031	6.64
	0.155	32.39
0.925	0.309	62.90
	0.464	92.63
	0.618	121.99
	0.773	151.78
	0.071	15.08
	0.141	29.79
	0.211	43.88
	0.282	57.85
	0.353	71.62
	0.423	85.20
0.950	0.494	98.70
	0.564	112.14
	0.635	125.63
	0.705	139.21
	0.776	153.02
	0.847	167.30
	0.917	182.57

[a] Corrected for truncation error.

TABLE X

COMPUTER DATA ON TWO-DIMENSIONAL FLOW THROUGH DEFORMABLE POROUS MEDIA

Mat Thickness = 1 inch Slot Width = 1/2 inch

Porosity (ε)	Relative Pressure Drop ($\Delta P_t / \Delta P_{Max}$)	Adjusted Flow Rate,[a] $Q/(K_{App} \cdot \Delta P_{Max}) \times 10^{-2}$, cm.
	0.011	2.24
	0.026	5.54
	0.053	11.00
	0.079	16.38
0.900	0.105	21.69
	0.158	32.13
	0.210	42.34
	0.316	61.34
	0.473	91.02
	0.031	6.53
	0.093	19.21
	0.185	37.60
0.925	0.309	61.21
	0.464	89.68
	0.618	117.45
	0.773	145.11
	0.927	174.01
	0.071	14.85
	0.141	29.06
	0.212	42.89
	0.282	56.40
	0.353	69.64
0.950	0.423	82.68
	0.494	95.56
	0.564	108.31
	0.635	121.01
	0.706	133.67
	0.776	146.43
	0.847	59.37

[a] Corrected for truncation error.

TABLE XI

COMPUTER DATA ON TWO-DIMENSIONAL FLOW THROUGH DEFORMABLE POROUS MEDIA

Mat Thickness = 1 inch Slot Width = 1/4 inch

Porosity (ϵ)	Relative Pressure Drop ($\Delta P_t / \Delta P_{Max}$)	Adjusted Flow Rate,[a] $Q/(K_{App} \cdot \Delta P_{Max}) \times 10^{-2}$, cm.
	0.011	2.19
	0.026	5.41
	0.053	10.71
	0.079	15.95
0.900	0.105	21.11
	0.158	31.24
	0.210	41.14
	0.316	60.35
	0.473	88.00
	0.031	6.38
	0.093	18.71
	0.185	36.56
0.925	0.309	59.39
	0.464	86.75
	0.618	113.23
	0.773	139.25
	0.927	165.70
	0.0705	14.54
	0.141	28.34
	0.212	41.74
	0.282	54.81
	0.353	67.57
0.950	0.423	80.12
	0.494	92.45
	0.564	104.65
	0.635	116.69
	0.706	128.65
	0.776	140.60
	0.847	152.62

[a] Corrected for truncation error.

TABLE XII

EXPERIMENTAL DATA ON TWO-DIMENSIONAL FLOW
THROUGH DEFORMABLE POROUS MEDIA

Mat Thickness = 1 inch		Slot Width = 1 inch	
Run 16	ε_I = 0.925	Run 18	ε_I = 0.908
$(\Delta P_t/\Delta P_{Max})$	$Q/(K_{App} \cdot \Delta P_{Max}) \times 10^{-2}$	$(\Delta P_t/\Delta P_{Max})$	$Q/(K_{App} \cdot \Delta P_{Max}) \times 10^{-2}$
0.0064	1.32	0.0052	1.24
0.0124	2.59	0.0148	3.31
0.0185	3.87	0.0257	5.44
0.0254	5.18	0.0377	7.92
0.0324	6.54	0.0474	9.05
0.0397	7.83	0.0594	11.70
0.0460	9.18	0.0778	14.94
0.0535	10.73	0.0926	17.94
0.0623	12.37	0.1093	21.09
0.0700	13.88	0.1291	24.49
0.0892	17.55	0.1307	24.73
0.1044	19.94	0.1476	28.39
0.1217	23.48	0.1592	30.66
0.1428	27.89	0.1757	34.03
0.1784	34.36	0.1887	37.44
0.2119	40.43	0.2006	39.25
0.2273	43.50	0.2150	44.04
0.2453	47.37	0.2296	47.56
0.2677	51.91		
0.2995	58.71		
0.3279	64.98		
0.3474	69.12		

TABLE XIII

EXPERIMENTAL DATA ON TWO-DIMENSIONAL FLOW
THROUGH DEFORMABLE POROUS MEDIA

Mat Thickness = 1 inch

Slot Width = 1 inch

Run 19	ε_I = 0.940	Run 20	ε_I = 0.901
$(\Delta P_t/\Delta P_{Max})$	$Q/(K_{App} \cdot \Delta P_{Max}) \times 10^{-2}$	$(\Delta P_t/\Delta P_{Max})$	$Q/(K_{App} \cdot \Delta P_{Max}) \times 10^{-2}$
0.012	3.14	0.0046	1.05
0.035	8.41	0.0090	2.10
0.059	13.81	0.0157	3.54
0.088	20.10	0.0226	5.00
0.118	25.45	0.0307	6.73
0.141	29.70	0.0409	8.76
0.174	36.03	0.0474	9.97
0.206	42.34	0.0514	10.61
0.241	49.10	0.0557	11.41
0.297	58.96	0.0591	12.12
0.305	60.09	0.0668	13.69
0.348	67.78	0.0727	15.07
0.391	75.40	0.0787	16.37
0.425	82.48	0.0854	17.71
0.458	88.12	0.0955	19.74
0.490	94.08	0.0966	19.98
0.536	103.94	0.1079	22.18
0.564	109.52	0.1160	23.80
0.594	115.76	0.1192	24.67
0.634	122.65		
0.666	129.68		
0.703	138.11		
0.697	137.07		

TABLE XIV

EXPERIMENTAL DATA ON TWO-DIMENSIONAL FLOW THROUGH DEFORMABLE POROUS MEDIA

Mat Thickness = 1 inch Slot Width = 1/2 inch

Run 22	ε_I = 0.938	Run 24	ε_I = 0.904
$(\Delta P_t/\Delta P_{Max})$	$Q/(K_{App} \cdot \Delta P_{Max}) \times 10^{-2}$	$(\Delta P_t/\Delta P_{Max})$	$Q/(K_{App} \cdot \Delta P_{Max}) \times 10^{-2}$
0.015	3.86	0.013	2.97
0.042	10.34	0.027	6.02
0.072	16.97	0.041	9.50
0.107	24.70	0.055	11.58
0.125	27.17	0.070	14.66
0.153	31.43	0.087	18.04
0.175	35.43	0.104	21.73
0.202	40.23	0.136	27.57
0.236	47.42	0.162	32.29
0.262	53.28	0.190	37.41
0.290	59.14	0.210	41.21
0.323	64.73	0.232	45.31
0.345	69.26	0.254	50.33
0.370	74.06	0.275	54.84
0.401	79.39	0.300	59.25
0.428	84.58	0.324	64.27
0.456	89.51	0.345	68.16
0.487	94.84	0.369	72.47
0.517	100.06	0.395	77.29
0.536	105.23		
0.555	108.69		
0.575	113.22		

TABLE XV

EXPERIMENTAL DATA ON TWO-DIMENSIONAL FLOW
THROUGH DEFORMABLE POROUS MEDIA

Mat Thickness = 1 inch

Run 25. ε_I = 0.920		Run 26 ε_I = 0.934	
Slot Width = 1/2 inch		Slot Width = 1/4 inch	
$(\Delta P_t / \Delta P_{Max})$	$Q/(K_{App} \cdot \Delta P_{Max}) \times 10^{-2}$	$(\Delta P_t / \Delta P_{Max})$	$Q/(K_{App} \cdot \Delta P_{Max}) \times 10^{-2}$
0.021	4.35	0.025	4.05
0.042	8.81	0.057	10.84
0.064	13.91	0.091	17.79
0.085	16.89	0.125	25.89
0.106	20.86	0.213	39.10
0.133	26.42	0.267	49.15
0.165	33.32	0.293	54.18
0.197	39.77	0.318	58.92
0.233	47.65	0.348	64.09
0.271	53.43	0.378	68.98
0.306	60.04	0.408	74.00
0.346	67.09	0.446	79.03
0.381	73.92	0.481	84.06
0.416	80.75	0.513	88.80
0.452	87.35	0.550	93.97
0.488	94.26	0.587	99.70
0.529	101.16	0.651	106.68
0.567	107.61		
0.604	113.32		
0.653	120.82		

TABLE XVI

EXPERIMENTAL DATA ON TWO-DIMENSIONAL FLOW
THROUGH DEFORMABLE POROUS MEDIA

Mat Thickness = 1 inch Slot Width = 1/4 inch

Run 27	ε_I = 0.885	Run 28	ε_I = 0.916
$(\Delta P_t/\Delta P_{Max})$	$Q/(K_{App} \cdot \Delta P_{Max}) \times 10^{-2}$	$(\Delta P_t/\Delta P_{Max})$	$Q/(K_{App} \cdot \Delta P_{Max}) \times 10^{-2}$
0.0055	1.31	0.010	2.42
0.015	3.49	0.027	6.47
0.026	5.73	0.049	10.62
0.039	8.34	0.074	15.46
0.049	10.08	0.092	20.60
0.066	13.41	0.138	27.36
0.078	15.75	0.175	33.45
0.099	19.89	0.209	39.53
0.121	23.85	0.237	44.02
0.145	27.90	0.268	48.36
0.168	31.86	0.297	53.33
0.191	36.09	0.324	57.93
0.213	39.96	0.355	62.52
0.237	44.19	0.388	67.53
0.260	48.15	0.418	72.18
0.285	52.83	0.448	77.15
0.305	55.98	0.487	84.09
0.333	60.12	0.509	86.91
0.359	64.36		